Decadal variability of ice-shelf melting in the Amundsen Sea driven by sea-ice freshwater fluxes

Michael Haigh[1] and Paul Richard Holland[1]

[1]British Antarctic Survey

January 22, 2024

Abstract

The ice streams flowing into the Amundsen Sea, West Antarctica, are losing mass due to changes in the oceanic basal melting of their floating ice shelves. Rapid ice-shelf melting is sustained by the delivery of warm Circumpolar Deep Water to the ice-shelf cavities, which is first supplied to the continental shelf by an undercurrent that flows eastward along the shelf break. Temporal variability of this undercurrent controls ice-shelf basal melt variability. Recent work shows that on decadal timescales the undercurrent variability opposes surface wind variability. Using a regional model, we show that undercurrent variability is driven by sea-ice freshwater fluxes, particularly those north of the shelf break, which affect the cross-shelf break density gradient. This sea-ice variability is caused by tropical Pacific variability impacting atmospheric conditions over the Amundsen Sea. Ice-shelf melting also feeds back onto the undercurrent by affecting the on-shelf density, thereby influencing shelf-break density gradient anomalies.

Decadal variability of ice-shelf melting in the Amundsen Sea driven by sea-ice freshwater fluxes

Michael Haigh[1] and Paul R. Holland[1]

[1]British Antarctic Survey, Cambridge, UK

Key Points:

- An undercurrent flowing along the Amundsen Sea shelf break regulates oceanic ice-shelf melting in the region.
- Model results have shown that decadal variability of the undercurrent opposes the wind variability.
- We show that sea-ice freshwater flux anomalies linked to tropical Pacific variability regulate the undercurrent and ice-shelf melting.

Corresponding author: Michael Haigh, `michai@bas.ac.uk`

Abstract

The ice streams flowing into the Amundsen Sea, West Antarctica, are losing mass due to changes in the oceanic basal melting of their floating ice shelves. Rapid ice-shelf melting is sustained by the delivery of warm Circumpolar Deep Water to the ice-shelf cavities, which is first supplied to the continental shelf by an undercurrent that flows eastward along the shelf break. Temporal variability of this undercurrent controls ice-shelf basal melt variability. Recent work shows that on decadal timescales the undercurrent variability opposes surface wind variability. Using a regional model, we show that undercurrent variability is driven by sea-ice freshwater fluxes, particularly those north of the shelf break, which affect the cross-shelf break density gradient. This sea-ice variability is caused by tropical Pacific variability impacting atmospheric conditions over the Amundsen Sea. Ice-shelf melting also feeds back onto the undercurrent by affecting the on-shelf density, thereby influencing shelf-break density gradient anomalies.

Plain Language Summary

The glaciers that flow towards the Amundsen Sea, West Antarctica, are losing ice faster than most others about the continent. Once these glaciers reach the coast, they extend out onto the ocean surface, forming ice shelves. The rapid loss of ice is caused by changes in melting by relatively warm ocean waters beneath the floating ice shelves. In the Amundsen Sea, a deep ocean current is responsible for delivering warm water from the deep ocean to the ice shelves. We present model results that show that this deep current varies on decadal timescales as a consequence of systematic sea-ice melt and formation patterns. A faster current drives more rapid ice shelf melting which, via a feedback process, further accelerates the current. Climate variability originating in the tropical Pacific Ocean is responsible for the variability in the sea-ice, and is therefore also responsible for the effects on melting of the ice shelves.

1 Introduction

Melting of the West Antarctic Ice Sheet provides Antarctica's biggest contribution to global sea-level rise (Shepherd et al., 2018), with the ice streams draining into the Amundsen Sea of particular concern (Mouginot et al., 2014; Rignot et al., 2014; Joughin et al., 2014). Rapid ice loss in this region is due to the access of warm Circumpolar Deep Water (CDW) to the undersides of the ice shelves, the floating extensions of the grounded ice streams (Jacobs et al., 1996; Dutrieux et al., 2014; Heywood et al., 2016). Ocean modelling studies suggest that this basal melting increased over the 20th century due to anthropogenic forcing (Naughten et al., 2022), and will continue to increase during the 21st century (Jourdain et al., 2022; Naughten et al., 2023). Superimposed on any such long-term trends are the impacts of strong natural decadal climate variability (Dutrieux et al., 2014; Jenkins et al., 2018), on which we focus in this study.

Access of CDW to the Amundsen Sea ice shelves is controlled by an undercurrent that flows along the continental shelf break. As observed (Walker et al., 2007, 2013; Assmann et al., 2013) and modelled (Thoma et al., 2008; Kimura et al., 2017; Webber et al., 2019; Caillet et al., 2022), the undercurrent flows eastward along the shelf break, and is diverted onto the continental shelf by bathymetric troughs intersecting the shelf break. Through this process the undercurrent transports warm CDW onto the continental shelf, which then flows across the shelf and beneath the ice shelves. Changes in the undercurrent control the variability of ice-shelf melting (Jenkins et al., 2016; Dotto et al., 2019, 2020) and are implicated in historical and future changes in melting (Naughten et al., 2022, 2023). Therefore, understanding drivers of undercurrent variability is essential for understanding future melt of the vulnerable ice streams in the Amundsen Sea region.

The undercurrent exists due to the Antarctic Slope Front (ASF), which separates CDW north of the shelf break from the lighter, cooler and fresher waters to the south (Jacobs, 1991; Stewart et al., 2019). This creates a south-to-north pressure gradient which causes the flow to be more eastward with depth. Variability in the ASF, or wider ocean density variability, will drive baroclinic (depth-dependent) variability in the undercurrent. The density structure across the shelf break can be affected by a number of processes, including wind-driven downwelling/upwelling (Spence et al., 2014), surface buoyancy fluxes (Caillet et al., 2022), and ice-shelf basal melting (Moorman et al., 2020; Si et al., 2023).

Winds drive barotropic (depth-independent) variability in the undercurrent by influencing gradients in sea-surface height, such that eastward wind anomalies drive an eastward acceleration in both the surface and deep flow (Assmann et al., 2013; Jenkins et al., 2016; Dotto et al., 2019, 2020). This is thought to be the dominant mechanism on short (synoptic to interannual) timescales (Wåhlin et al., 2013; Silvano et al., 2022). However, the Amundsen Sea is impacted slower natural and anthropogenic climate changes that vary on interannual, interdecadal, and centennial timescales (Steig et al., 2012; Li et al., 2021; Holland et al., 2019, 2022). Recently, Silvano et al. (2022) presented regional model output showing that undercurrent variability actually opposes surface wind variability on decadal timescales, such that eastward (westward) shelf-break wind anomalies coincide with a weaker (stronger) eastward undercurrent, while the surface flow variability simply follows the winds. Silvano et al. (2022) hypothesised that this was due to wind-driven upwelling/downwelling anomalies on the continental shelf driving slow baroclinic variability that outweighs the faster barotropic effects of the shelf-break winds. In this study we examine the same regional model and demonstrate that this decadal baroclinic variability is in fact driven by sea-ice and ice-shelf freshwater fluxes.

2 Methods

2.1 Amundsen Sea regional model

Following Silvano et al. (2022), we use the Massachusetts Institute of Technology general circulation model (MITgcm) including ocean, sea-ice and ice-shelf components, with the same configuration as Naughten et al. (2022) with one minor difference in the application of iceberg meltwater. The model domain spans the longitudes 140°W to 80°W and latitudes 75.5°S to 62°S. The lateral grid resolution is 0.1° in longitude, corresponding to an isotropic grid spacing of ~ 2.75 km in the south and ~ 5.15 km in the north. The vertical direction is discretised by 50 levels with the thinnest (10 m) levels near the surface and the thickest (200 m) levels near the ocean bottom. The model is forced by six-hourly ERA5 (Hersbach et al., 2020) 10 m winds, surface longwave and shortwave radiation, 2 m air temperature, 2 m specific humidity, precipitation and atmospheric pressure. The model is spun up using the 1979-2002 interval of the external forcing data. After this spinup, the forcing is restarted from 1979 and the model is run until 2019 with monthly mean output. Our analysis is based on model output during 1984-2019. Further details of the model can be found in Naughten et al. (2022).

2.2 Definition of the undercurrent

The eastward undercurrent is defined using an approach very similar to Silvano et al. (2022). We start by locating the 1000 m isobath at the shelf break between 125°W and 108°W, the undercurrent longitudes of interest. For each longitude along the isobath, the along-slope flow beneath the 1028 kg m^{-3} isopycnal and above 800 m depth is averaged over a meridional range of three grid points either side of the isobath. The undercurrent speed is then defined as the maximum of these meridionally averaged values at any depth, which typically occurs near 500 m depth. The along-slope surface current and winds are computed at each longitude as an average over the same meridional range. All quantities are then averaged along the undercurrent pathway, with the Dotson-Getz and Pine Island-Thwaites West troughs excluded from the computations. Similar to Silvano et al. (2022), we find that using alternate undercurrent definitions does not affect our conclusions.

2.3 Statistical methods

We use a combination of correlations and composites to analyse model output. For correlations we use the Pearson correlation coefficient r and significance p, the latter computed using a two-sided Student's t-test. When computing the significance we account for the effective degrees of freedom, defined as the number of time samples divided by twice the e-folding decorrelation timescale. Doing this is important since we focus on decadal variability, but have model output spanning only a few decades. For the same reason, not all provided correlations are significant at the 95% level. Significance values will be provided with each correlation coefficient.

For composites of a response field against a scalar predictor, the positive (negative) composite is computed by averaging anomalies of the response field over all months for which the predictor is half a standard deviation greater (less) than its mean. We use two predictors: the undercurrent speed timeseries described above, and the Tripole Index (TPI) of the Interdecadal Pacific Oscillation (IPO).

We use the TPI as a means to quantify the influence of tropical Pacific variability, which dominates variability in the Amundsen Sea (Steig et al., 2012; Dutrieux et al., 2014; Li et al., 2021). Previous studies have separated this variability into two modes: El Niño-Southern Oscillation (ENSO) on shorter timescales and the IPO on longer (>13-year) timescales (Newman et al., 2016; Li et al., 2021). The monthly TPI is designed to quantify the longer IPO variability (Henley et al., 2015), but is also highly correlated to all ENSO indices (Holland et al., 2019). Since the timescale under consideration here is intermediate between ENSO and IPO, we use the monthly TPI index to represent all Pacific variability, without ascribing the variability to either mode. In this study, this index and all other timeseries are detrended, deseasoned and have a 5-year running mean applied. The only exception is in section 3.3, where we consider tropical Pacific impacts on wintertime atmospheric fields over the Amundsen Sea.

3 Results

3.1 The Amundsen Sea undercurrent

Fig. 1a shows the time-mean (1984-2019) flow and potential temperature at 455 m depth in the Amundsen Sea. Consistent with observations (Walker et al., 2007, 2013), the eastward undercurrent follows the continental slope and is guided southwards onto the shelf by bathymetric troughs at the shelf break. Through this process, warm CDW is advected onto the continental shelf, and eventually towards the ice shelves.

Fig. 1b shows timeseries of the along-slope undercurrent, surface current, surface winds and the ice-shelf basal melt integrated over all the ice shelves shown in Fig. 1a. Getz Ice Shelf west of 125°W is omitted from this computation since this part of its cavity is not supplied with CDW by the undercurrent. As first reported by Silvano et al. (2022), on decadal timescales the undercurrent is anticorrelated with the surface current ($r = -0.62$, $p = 0.09$) and weakly anticorrelated with the winds ($r = -0.26$, $p = 0.48$). The role of the undercurrent in controlling the ice-shelf basal melt is reflected in the strong positive correlation ($r = 0.96$, $p < 0.05$) between these two timeseries.

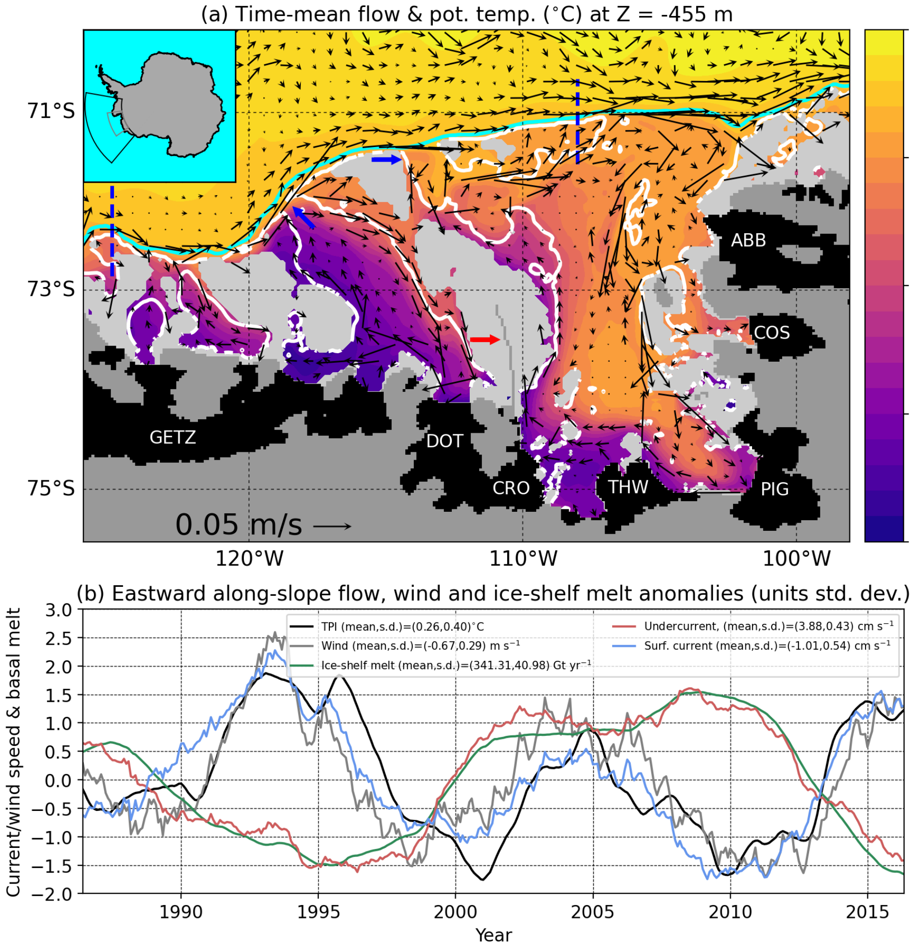

Figure 1. (a) Time-mean (1984-2019) flow (arrows, every six grid points) and potential temperature (colour, °C) at 455 m depth from model output. The cyan (white) contour represents the 1000 m (500 m) isobath. Light grey masking represents bathymetry shallower than 455 m, dark grey masking represents land and black masking represents the ice shelves (GETZ=Getz, DOT=Dotson, CRO=Crosson, THW=Thwaites, PIG=Pine Island Glacier, COS=Cosgrove, ABB=Abbot). Blue arrows indicate the Dotson-Getz and Pine Island-Thwaites West troughs. The red arrow indicates Bear Ridge, on which grounded icebergs sit (Bett et al., 2020). Inset: map showing model domain (black box) and subregion shown in this figure (grey box). (b) Timeseries of along-slope undercurrent, surface current, winds, area-integrated ice-shelf basal melt and TPI. Timeseries are demeaned and normalised by their standard deviations (see legend).

3.2 Density anomalies and freshwater fluxes

Fig. 2a shows the time-mean cross-slope density and along-slope velocity averaged along the undercurrent pathway, with y-coordinate centered on the 1000 m isobath. The southward deepening of density contours over the shelf break represents the ASF. Although the ASF is typically weaker in the Amundsen Sea compared to other sectors about Antarctica, it is nonetheless strong enough for the time-mean flow to transition from weak westward flow near the surface to strong eastward ($\sim$ 5 cm s^{-1}) flow at 300–500 m depth.

Figs. 2c,e show composites using the undercurrent speed as the predictor and the along-slope velocity and cross-slope density as the response fields. Eastward undercurrent anomalies coincide with negative density anomalies on the continental shelf that span most of the water column, and positive density anomalies north of the shelf break concentrated in the top 50 m of the water column. Density anomalies with the same spatial distribution but opposite sign are diagnosed for westward undercurrent anomalies. Cross-slope pressure gradient anomalies (not shown) very closely resemble undercurrent anomalies, confirming that the undercurrent decadal variability is both geostrophic and caused by these density anomalies.

We now consider winds and freshwater fluxes, both potential drivers of the density and undercurrent variability. Fig. 2b shows the time-mean winds, sea-ice freshwater flux (positive values freshen the ocean), and ice-shelf freshwater flux. Fig. 2d,f shows composites of the freshwater flux and wind responses to the undercurrent speed predictor. The wind composites can be used to test the hypothesis of Silvano et al. (2022), i.e., that anomalous wind-driven upwelling/downwelling on the continental shelf drives the undercurrent variability. Coastal wind anomalies tend to be weak and, importantly, are not oriented in the direction required to support this hypothesis. For example, during eastward undercurrent anomalies, coastal wind anomalies are predominantly eastward and induce coastal upwelling anomalies which would weaken, rather than strengthen, the shelf-break baroclinicity/undercurrent. Composites of the wind stress curl anomaly response to the undercurrent predictor (Fig. S1) also suggest that wind-driven upwelling/downwelling does not drive the undercurrent variability. Therefore, with the conclusion that wind-driven effects are not responsible for the decadal variability, we move on to consider freshwater fluxes.

The composites in Fig. 2d,f illustrate how freshwater flux anomalies drive the density and undercurrent variability (Fig. 2c,e). North of the shelf break, relatively dense (light) surface waters that contribute to eastward (westward) undercurrent anomalies are a result of anomalous sea-ice-driven salinification (freshening). The on-shelf density anomalies, which have sign opposite to those off-shelf, are predominantly due to ice-shelf freshwater flux variability. We propose that this ice-shelf melt variability is initially a response to the undercurrent variability driven by sea-ice freshwater fluxes. Then a positive feedback between the undercurrent and ice-shelf melting is initiated, whereby ice-shelf meltwater anomalies impact the on-shelf density and shelf-break density gradient, reinforcing undercurrent anomalies. Over time, the on-shelf density anomalies extrude off of the continental shelf, leading to a reduction the in cross-shelf density gradient anomalies that had previously built up.

During eastward undercurrent anomalies, on-shelf sea-ice freshwater flux anomalies (Fig. 2d) have opposite sign to those off-shelf, especially in coastal areas and near Bear Ridge (red arrow, Fig 1a), further contributing to the cross-slope density gradient anomaly. During westward undercurrent anomalies, however, on-shelf sea-ice freshwater flux anomalies (Fig. 2f) do not have a distinct spatial pattern.

More evidence of the mechanism by which freshwater fluxes drive undercurrent variability is provided by idealised modelling results (Figs. S2 and S3) using the MITgcm configuration of Haigh et al. (2023). In these simulations, decadally varying surface fresh-

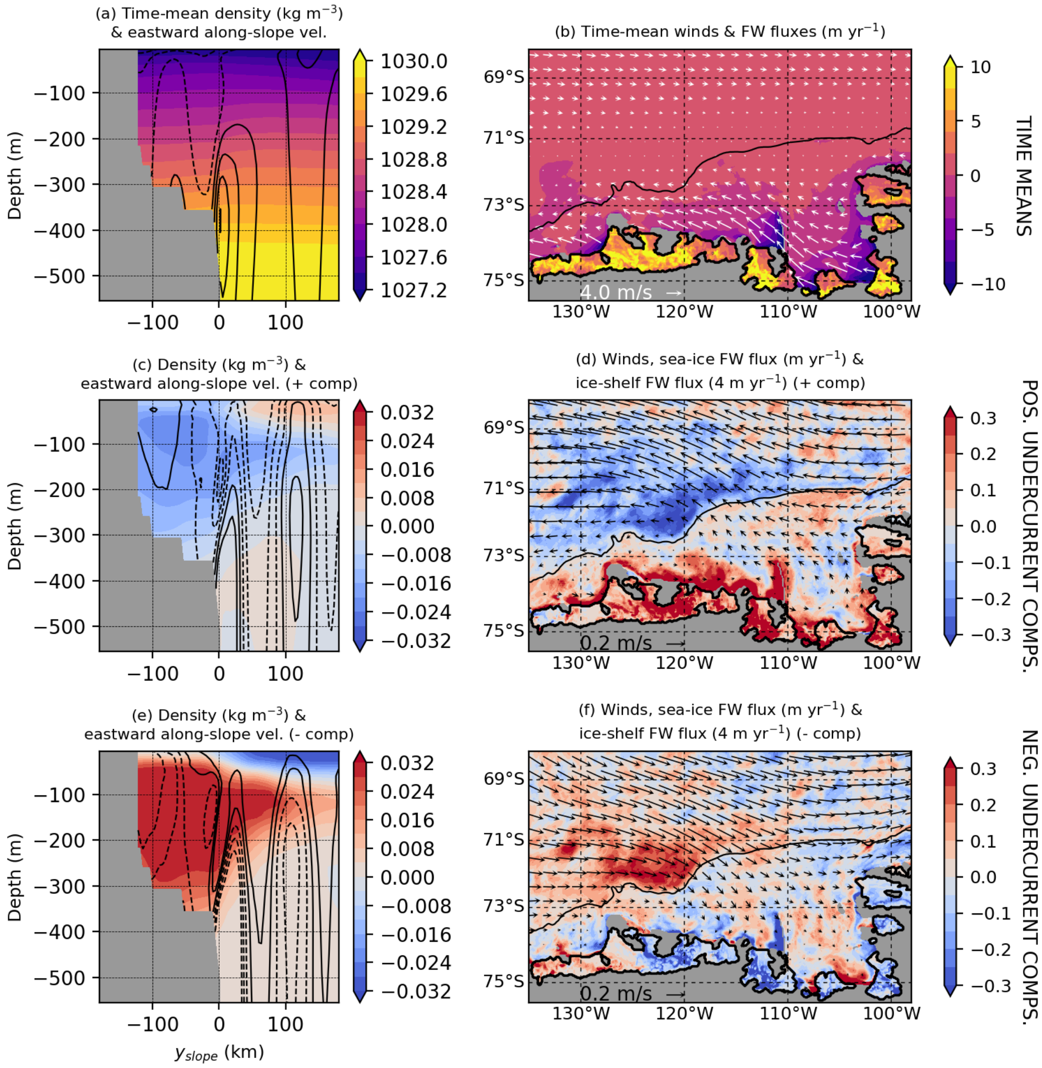

Figure 2. (a) Time-mean density (colour, kg m^{-3}) and eastward along-slope velocity (contours, 1 cm s^{-1} contour interval, dashed are zero and negative) averaged along the undercurrent pathway. (b) Time-mean winds (arrows) and sea-ice and ice-shelf freshwater fluxes (colour, m yr^{-1}). (c,e) Composites of density and eastward along-slope velocity (1 mm s^{-1} contour interval) for eastward/westward undercurrent anomalies. (d,f) Composites of sea-ice freshwater fluxes (m yr^{-1}), ice-shelf freshwater fluxes (4 m yr^{-1}) and winds for eastward/westward undercurrent anomalies. In (b,d,f) the thick black contour outlines the ice-shelf drafts and the thin black contour is the 1000 m shelf-break isobath.

water fluxes are applied and are shown to drive a decadally varying undercurrent by impacting the cross-shelf break density gradient.

Fig. 3a shows a correlation map with the undercurrent strength as predictor and sea-ice and ice-shelf freshwater fluxes as response fields, further quantifying the mechanism by which freshwater fluxes drive decadal variability in the undercurrent. The undercurrent negatively correlates ($r \approx 0.8$, $p < 0.05$) with sea-ice freshening anomalies north of the shelf break, but not those downstream of the undercurrent longitudes (east of 108°W). The undercurrent positively correlates (not significant) with sea-ice freshening anomalies over most of the continental shelf, in particular near Bear Ridge and in front of Getz ice shelf. Strong positive correlations ($r \approx 0.9$, $p < 0.05$) between the undercurrent and ice-shelf basal melt are suggestive of the feedback mechanism that exists between the two.

Fig. 3b shows timeseries of the sea-ice freshwater flux anomalies, integrated over the on-shelf and off-shelf regions shown in Fig. 3a. These regions are selected such that they span the same longitudes and have the same area. Also shown in Fig 3b are timeseries of the difference between the on-shelf and off-shelf freshwater flux anomalies, and the area-integrated ice-shelf freshwater flux anomaly. We exclude the western half of Getz Ice Shelf from the latter integral since it is not supplied with CDW by the undercurrent, although its meltwater may still impact the undercurrent. These timeseries are not sensitive to the precise choice of the areas of integration. The negation of the off-shelf flux anomaly is shown so that, for all timeseries, positive values correspond to an eastward acceleration of the undercurrent.

Apparently by coincidence, area-integrated ice-shelf and sea-ice freshwater flux anomalies have a very similar magnitude (Bett et al., 2020), suggesting that they make similar contributions to the undercurrent decadal variability. The undercurrent negatively correlates with the off-shelf sea-ice freshwater flux ($r = -0.69$, $p < 0.05$), does not notably correlate with the on-shelf sea-ice freshwater flux ($r = 0.20$, $p = 0.62$), but does notably correlate with their difference ($r = 0.71$, $p = 0.08$). These correlations reflect how the integrated off-shelf sea-ice freshwater flux has a distinct decadal variability similar to the undercurrent, whereas the on-shelf sea-ice freshwater flux does not (Fig 3b).

3.3 The role of tropical Pacific variability

While decadal variability in the ice-shelf basal melt is attributed to the undercurrent, the driver of decadal variability in the sea-ice freshwater fluxes remains to be determined. Here we attribute sea-ice freshwater flux variability to tropical Pacific variability, as quantified by the TPI (section 2.3). Positive (negative) phases of ENSO and the IPO are typically associated with a filled (deepened) Amundsen Sea Low (ASL) (Lachlan-Cope & Connolley, 2006; Clem et al., 2019; Li et al., 2021). This corresponds to eastward (westward) wind anomalies at the shelf break, which explains the decadal variability of the along-shelf break surface flow (Silvano et al., 2022) and its correlation with the TPI ($r = 0.91$, $p < 0.05$; Fig. 1b).

The negative correlation between the undercurrent and the TPI ($r = -0.63$, $p = 0.07$; Fig. 1b) is found to be caused by the impacts of Pacific variability on atmospheric conditions over the Amundsen Sea during austral winter (JJA), the season during which tropical teleconnections with the region are strongest (Ding et al., 2011; Li et al., 2021). Fig. 4a,b shows composites of the winter sea-ice freshwater flux anomaly during positive and negative phases of the TPI. Similar to the relationship between freshwater fluxes and undercurrent speed (Figs. 2 and 3), there is anomalous sea-ice-driven freshening (salinification) north of the shelf break during positive (negative) composites of the TPI. The spatial distribution of the on-shelf sea-ice freshwater flux anomaly is less distinct, and its sign tends to follow the anomaly north of the shelf break.

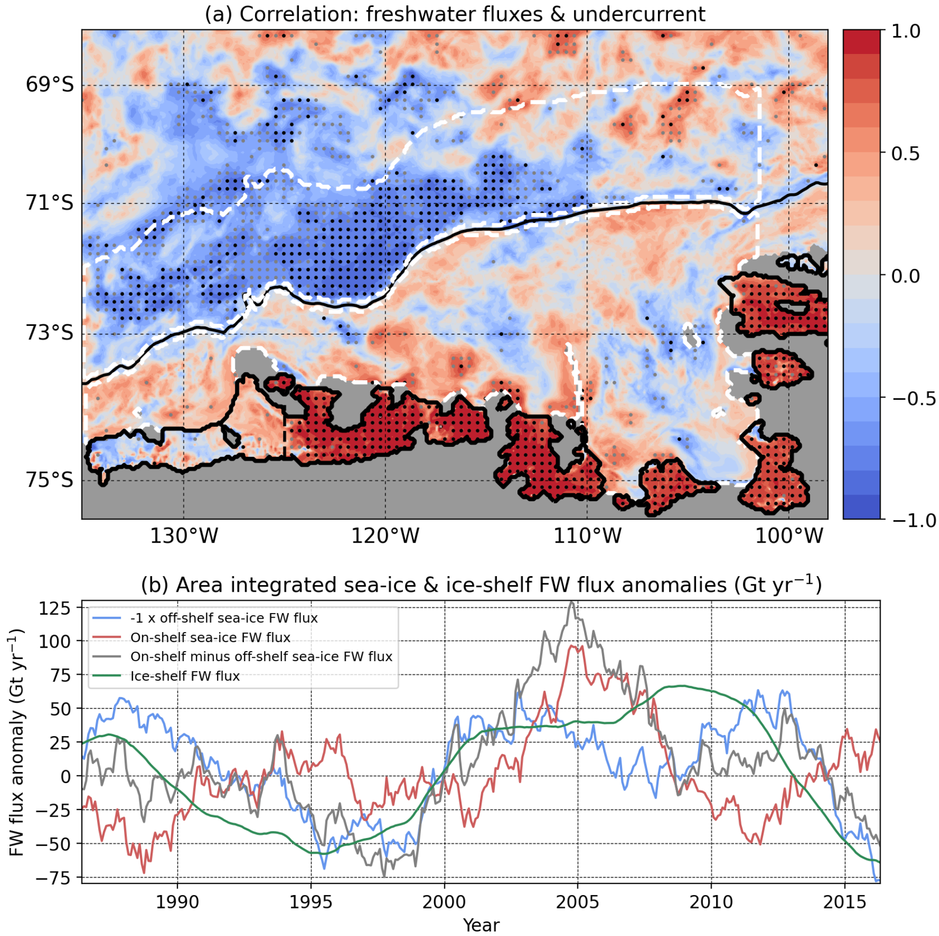

Figure 3. (a) Correlation between the undercurrent speed and the sea-ice and ice-shelf freshwater fluxes into the ocean. Black (grey) stippling denotes significance $p < 0.05$ ($p < 0.15$). The thick black contour outlines the ice-shelf drafts and the thin black contour is the 1000 m shelf-break isobath. (b) Timeseries of area-integrated freshwater flux anomalies (Gt yr^{-1}), oriented such that positive values strengthen the undercurrent. Plotted are the on-shelf sea-ice freshwater flux anomaly (red), the negation of the off-shelf sea-ice freshwater flux anomaly (blue), the on-shelf minus off-shelf sea-ice freshwater fluxes (grey) and the ice-shelf freshwater flux anomaly (green). Areas of integration for the sea-ice freshwater fluxes are outlined by the white contours in panel (a). The ice-shelf freshwater flux is integrated over all ice shelves shown in panel (a), excluding the area of the Getz Ice Shelf west of 125°W.

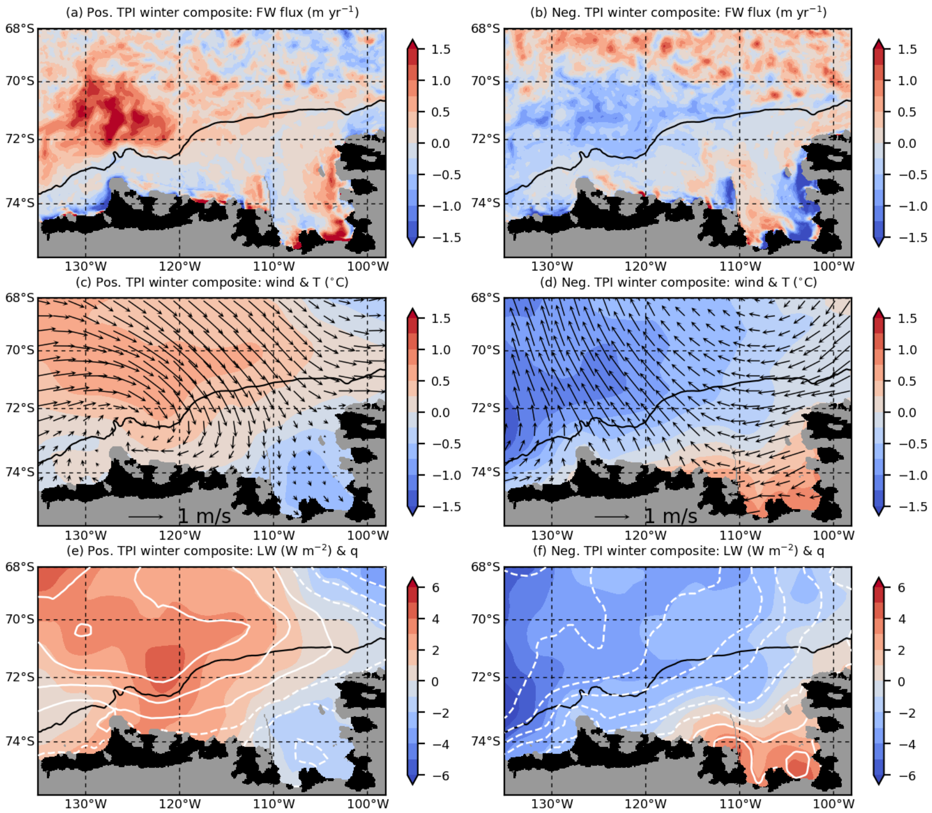

Figure 4. Winter (JJA) composites using the TPI as the predictor and freshwater fluxes and atmospheric conditions as the response fields. (a,b) Composites of the winter sea-ice freshwater flux anomaly (m yr^{-1}) during positive/negative TPI. (c,d) Composites of the winter 10 m wind (arrows) and 2 m air temperature, T (colour, °C) during positive/negative TPI. (e,f) Composites of the winter downward longwave radiation (colour, W m^{-2}) and 2 m specific humidity, q (white contours, 2.5×10^{-5} kg kg^{-1} contour interval, dashed are zero and negative) during positive/negative TPI.

Figs. 4c,d show composites of the ERA5 10 m winds and 2 m air temperature responses to the TPI predictor, and Figs. 4e,f show composites of the downward longwave (LW) radiation and 2 m specific humidity responses. During positive phases of the TPI, the weakened ASL creates northerly wind anomalies over the deep ocean. This transports relatively warm and moist air southwards over the region north of the shelf break, leading to greater downward LW radiation. As such, during positive phases of the TPI, all of the wintertime sea-ice surface heat fluxes (sensible and latent heat fluxes and LW radiation) are anomalously downwards, leading to a reduction in sea-ice formation and even periods of absolute sea-ice melt north of the shelf break. During negative phases of the TPI the opposite process occurs, causing greater sea-ice formation north of the shelf break.

For a given phase of the TPI, anomalies in thermodynamic atmospheric fields on the continental shelf have the opposite sign to anomalies north of the shelf break. However, freshwater flux anomalies on the continental shelf tend to have the same sign as anomalies north of the shelf break. This behaviour can be explained by winds near the coast: during negative phases of the TPI, wind anomalies tend to be directed away from the coast, opening coastal polynyas, forming more sea ice and driving greater brine rejection. During positive TPI phases, the opposite process occurs, although the coastal wind anomalies are weaker. The contrasting effects of coastal winds and thermodynamic atmospheric anomalies cause the indistinct spatial distribution of the on-shelf sea-ice freshwater fluxes and also cause the lack of distinct decadal variability compared to the off-shelf fluxes (Fig. 3b). These contrasting effects are also reflected by the weak correlation between the TPI and the on-shelf sea-ice freshwater fluxes ($r = 0.33$, $p = 0.39$) relative to the correlation between the TPI and the off-shelf fluxes ($r = 0.53$, $p = 0.15$).

4 Discussion and Conclusions

Understanding the variability of the Amundsen Sea eastward undercurrent is of great importance since it modulates basal melting of the ice shelves in the region. Until recently the undercurrent was thought to simply vary with the winds over the continental shelf break. However, Silvano et al. (2022) recently presented model results showing that on decadal timescales the undercurrent variability actually opposes wind variability. In this study we show that this undercurrent decadal variability is driven by a combination of sea-ice and ice-shelf freshwater fluxes.

Composites of our regional model output show that on decadal timescales eastward (westward) undercurrent anomalies are due to anomalous sea-ice-driven salinification (freshening) north of the shelf break which enhances (weakens) the cross-slope baroclinicity. Decadal variability in the sea-ice freshwater flux is due to tropical Pacific variability and its impact on the ASL during winter (Lachlan-Cope & Connolley, 2006; Clem et al., 2019; Li et al., 2021). During positive (negative) phases of the TPI, northerly (southerly) wind anomalies transport relatively warm and moist (cold and dry) air to the area north of the shelf break. The associated downward (upward) heat flux anomalies drive the diagnosed sea-ice freshening (salinification) anomalies. Periods of faster (slower) undercurrent lead to enhanced (reduced) ice-shelf basal melt. These ice-shelf basal melt anomalies create on-shelf density anomalies which reinforce the anomalies in the cross-slope pressure gradient (Moorman et al., 2020; Si et al., 2023) and undercurrent.

Our results are consistent with the simulations of Caillet et al. (2022), who perturb precipitation and air temperature over the Amundsen Sea continental shelf. These perturbations lead to surface buoyancy flux anomalies which impact the on-shelf density and induce undercurrent anomalies via the same mechanism as in this study. While Caillet et al. (2022) discussed buoyancy fluxes on the continental shelf, our results show that fluxes over the deep ocean are important for the Amundsen Sea undercurrent and ice shelves.

The conclusions of our study are based on one regional model simulation spanning just two periods of the decadal variability. For this reason presented timeseries have few effective degrees of freedom, meaning some provided correlations are not significant at the 95% level. For example, while the correlation between the undercurrent and off-shelf sea-ice freshwater flux is significant ($r = -0.69$, $p < 0.05$), the correlation between the TPI and the off-shelf fluxes ($r = 0.53$, $p = 0.15$) is not. Therefore, there is confidence in the link between the freshwater fluxes and the undercurrent, but further modelling efforts are necessary to gain more confidence in the link to tropical Pacific variability.

In this study we have focussed on natural decadal variability. However, the Amundsen Sea region is impacted by anthropogenic effects, driving trends in the regional winds (Goyal et al., 2021; Holland et al., 2022) which can drive trends in ocean conditions, in particular increasing the on-shelf heat content (Spence et al., 2014; Naughten et al., 2022). Climate projections show that ice-shelf basal melt in the Amundsen Sea is expected to increase over the next century (Jourdain et al., 2022; Naughten et al., 2023), a trend on which the decadal variability considered here is superimposed. Improving our understanding of both the anthropogenic trends and the natural variability remains a crucial challenge which must be tackled for society to mitigate against and adapt to future sea-level rise.

Data Availability Statement

The data and post-processing codes used in this study are available for download from Haigh and Holland (2024). Data for the Tripole Index (Henley et al., 2015) for the Interdecadal Pacific Oscillation can be found at https://psl.noaa.gov/data/timeseries/IPOTPI/.

Acknowledgments

This research was funded by the NERC project "Drivers of Oceanic Change in the Amundsen Sea", NE/T012803/1.

References

Assmann, K. M., Jenkins, A., Shoosmith, D. R., Walker, D. P., Jacobs, S. S., & Nicholls, K. W. (2013, dec). Variability of Circumpolar Deep Water transport onto the Amundsen Sea Continental shelf through a shelf break trough. *Journal of Geophysical Research: Oceans*, *118*(12), 6603–6620. doi: 10.1002/2013jc008871

Bett, D. T., Holland, P. R., Garabato, A. C. N., Jenkins, A., Dutrieux, P., Kimura, S., & Fleming, A. (2020, sep). The Impact of the Amundsen Sea Freshwater Balance on Ocean Melting of the West Antarctic Ice Sheet. *Journal of Geophysical Research: Oceans*, *125*(9). doi: 10.1029/2020jc016305

Caillet, J., Jourdain, N. C., Mathiot, P., Hellmer, H. H., & Mouginot, J. (2022, December). Drivers and Reversibility of Abrupt Ocean State Transitions in the Amundsen Sea, Antarctica. *Journal of Geophysical Research: Oceans*, *128*(1). doi: 10.1029/2022jc018929

Clem, K. R., Lintner, B. R., Broccoli, A. J., & Miller, J. R. (2019, June). Role of the South Pacific Convergence Zone in West Antarctic Decadal Climate Variability. *Geophysical Research Letters*, *46*(12), 6900–6909. doi: 10.1029/2019gl082108

Ding, Q., Steig, E. J., Battisti, D. S., & Küttel, M. (2011, April). Winter warming in West Antarctica caused by central tropical Pacific warming. *Nature Geoscience*, *4*(6), 398–403. doi: 10.1038/ngeo1129

Dotto, T. S., Garabato, A. C. N., Bacon, S., Holland, P. R., Kimura, S., Firing, Y. L., . . . Jenkins, A. (2019, nov). Wind-Driven Processes Controlling Oceanic

Heat Delivery to the Amundsen Sea, Antarctica. *Journal of Physical Oceanography*, *49*(11), 2829–2849. doi: 10.1175/jpo-d-19-0064.1

Dotto, T. S., Garabato, A. C. N., Wåhlin, A. K., Bacon, S., Holland, P. R., Kimura, S., … Jenkins, A. (2020, aug). Control of the Oceanic Heat Content of the Getz-Dotson Trough, Antarctica, by the Amundsen Sea Low. *Journal of Geophysical Research: Oceans*, *125*(8). doi: 10.1029/2020jc016113

Dutrieux, P., Rydt, J. D., Jenkins, A., Holland, P. R., Ha, H. K., Lee, S. H., … Schröder, M. (2014, jan). Strong Sensitivity of Pine Island Ice-Shelf Melting to Climatic Variability. *Science*, *343*(6167), 174–178. doi: 10.1126/science.1244341

Goyal, R., Gupta, A. S., Jucker, M., & England, M. H. (2021, feb). Historical and Projected Changes in the Southern Hemisphere Surface Westerlies. *Geophysical Research Letters*, *48*(4). doi: 10.1029/2020gl090849

Haigh, M., & Holland, P. R. (2024). *Data for Decadal variability of ice-shelf melt in the Amundsen Sea driven by freshwater fluxes.* Zenodo. doi: 10.5281/ZENODO.10391364

Haigh, M., Holland, P. R., & Jenkins, A. (2023, May). The Influence of Bathymetry Over Heat Transport Onto the Amundsen Sea Continental Shelf. *Journal of Geophysical Research: Oceans*, *128*(5). doi: 10.1029/2022jc019460

Henley, B. J., Gergis, J., Karoly, D. J., Power, S., Kennedy, J., & Folland, C. K. (2015, March). A Tripole Index for the Interdecadal Pacific Oscillation. *Climate Dynamics*, *45*(11–12), 3077–3090. doi: 10.1007/s00382-015-2525-1

Hersbach, H., Bell, B., Berrisford, P., Hirahara, S., Horányi, A., Muñoz-Sabater, J., … Thépaut, J. (2020, June). The ERA5 global reanalysis. *Quarterly Journal of the Royal Meteorological Society*, *146*(730), 1999–2049. doi: 10.1002/qj.3803

Heywood, K., Biddle, L., Boehme, L., Dutrieux, P., Fedak, M., Jenkins, A., … Webber, B. (2016, dec). Between the Devil and the Deep Blue Sea: The Role of the Amundsen Sea Continental Shelf in Exchanges Between Ocean and Ice Shelves. *Oceanography*, *29*(4), 118–129. doi: 10.5670/oceanog.2016.104

Holland, P. R., Bracegirdle, T. J., Dutrieux, P., Jenkins, A., & Steig, E. J. (2019, aug). West Antarctic ice loss influenced by internal climate variability and anthropogenic forcing. *Nature Geoscience*, *12*(9), 718–724. doi: 10.1038/s41561-019-0420-9

Holland, P. R., O'Connor, G. K., Bracegirdle, T. J., Dutrieux, P., Naughten, K. A., Steig, E. J., … Smith, J. A. (2022, December). Anthropogenic and internal drivers of wind changes over the Amundsen Sea, West Antarctica, during the 20th and 21st centuries. *The Cryosphere*, *16*(12), 5085–5105. doi: 10.5194/tc-16-5085-2022

Jacobs, S. S. (1991, nov). On the nature and significance of the Antarctic Slope Front. *Marine Chemistry*, *35*(1-4), 9–24. doi: 10.1016/s0304-4203(09)90005-6

Jacobs, S. S., Hellmer, H. H., & Jenkins, A. (1996, may). Antarctic Ice Sheet melting in the southeast Pacific. *Geophysical Research Letters*, *23*(9), 957–960. doi: 10.1029/96gl00723

Jenkins, A., Dutrieux, P., Jacobs, S., Steig, E., Gudmundsson, H., Smith, J., & Heywood, K. (2016, dec). Decadal Ocean Forcing and Antarctic Ice Sheet Response: Lessons from the Amundsen Sea. *Oceanography*, *29*(4), 106–117. doi: 10.5670/oceanog.2016.103

Jenkins, A., Shoosmith, D., Dutrieux, P., Jacobs, S., Kim, T. W., Lee, S. H., … Stammerjohn, S. (2018, aug). West Antarctic Ice Sheet retreat in the Amundsen Sea driven by decadal oceanic variability. *Nature Geoscience*, *11*(10), 733–738. doi: 10.1038/s41561-018-0207-4

Joughin, I., Smith, B. E., & Medley, B. (2014, may). Marine Ice Sheet Collapse Potentially Under Way for the Thwaites Glacier Basin, West Antarctica. *Science*, *344*(6185), 735–738. doi: 10.1126/science.1249055

Jourdain, N. C., Mathiot, P., Burgard, C., Caillet, J., & Kittel, C. (2022, November). Ice Shelf Basal Melt Rates in the Amundsen Sea at the End of the 21st Century. *Geophysical Research Letters*, *49*(22). doi: 10.1029/2022gl100629

Kimura, S., Jenkins, A., Regan, H., Holland, P. R., Assmann, K. M., Whitt, D. B., … Dutrieux, P. (2017, dec). Oceanographic Controls on the Variability of Ice-Shelf Basal Melting and Circulation of Glacial Meltwater in the Amundsen Sea Embayment, Antarctica. *Journal of Geophysical Research: Oceans*, *122*(12), 10131–10155. doi: 10.1002/2017jc012926

Lachlan-Cope, T., & Connolley, W. (2006, December). Teleconnections between the tropical Pacific and the Amundsen-Bellinghausens Sea: Role of the El Niño/Southern Oscillation. *Journal of Geophysical Research: Atmospheres*, *111*(D23). doi: 10.1029/2005jd006386

Li, X., Cai, W., Meehl, G. A., Chen, D., Yuan, X., Raphael, M., … Song, C. (2021, August). Tropical teleconnection impacts on Antarctic climate changes. *Nature Reviews Earth & Environment*, *2*(10), 680–698. doi: 10.1038/s43017-021-00204-5

Moorman, R., Morrison, A. K., & McC. Hogg, A. (2020, August). Thermal Responses to Antarctic Ice Shelf Melt in an Eddy-Rich Global Ocean–Sea Ice Model. *Journal of Climate*, *33*(15), 6599–6620. doi: 10.1175/jcli-d-19-0846.1

Mouginot, J., Rignot, E., & Scheuchl, B. (2014, mar). Sustained increase in ice discharge from the Amundsen Sea Embayment, West Antarctica, from 1973 to 2013. *Geophysical Research Letters*, *41*(5), 1576–1584. doi: 10.1002/2013gl059069

Naughten, K. A., Holland, P. R., & De Rydt, J. (2023, October). Unavoidable future increase in West Antarctic ice-shelf melting over the twenty-first century. *Nature Climate Change*, *13*(11), 1222–1228. doi: 10.1038/s41558-023-01818-x

Naughten, K. A., Holland, P. R., Dutrieux, P., Kimura, S., Bett, D. T., & Jenkins, A. (2022, mar). Simulated Twentieth-Century Ocean Warming in the Amundsen Sea, West Antarctica. *Geophysical Research Letters*, *49*(5). doi: 10.1029/2021gl094566

Newman, M., Alexander, M. A., Ault, T. R., Cobb, K. M., Deser, C., Di Lorenzo, E., … Smith, C. A. (2016, June). The Pacific Decadal Oscillation, Revisited. *Journal of Climate*, *29*(12), 4399–4427. doi: 10.1175/jcli-d-15-0508.1

Rignot, E., Mouginot, J., Morlighem, M., Seroussi, H., & Scheuchl, B. (2014, may). Widespread, rapid grounding line retreat of Pine Island, Thwaites, Smith, and Kohler glaciers, West Antarctica, from 1992 to 2011. *Geophysical Research Letters*, *41*(10), 3502–3509. doi: 10.1002/2014gl060140

Shepherd, A., Ivins, E., Rignot, E., Smith, B., van den Broeke, M., Velicogna, I., … others (2018, jun). Mass balance of the Antarctic Ice Sheet from 1992 to 2017. *Nature*, *558*(7709), 219–222. doi: 10.1038/s41586-018-0179-y

Si, Y., Stewart, A. L., & Eisenman, I. (2023, May). Heat transport across the Antarctic Slope Front controlled by cross-slope salinity gradients. *Science Advances*, *9*(18). doi: 10.1126/sciadv.add7049

Silvano, A., Holland, P. R., Naughten, K. A., Dragomir, O., Dutrieux, P., Jenkins, A., … Naveira Garabato, A. C. (2022, December). Baroclinic Ocean Response to Climate Forcing Regulates Decadal Variability of Ice-Shelf Melting in the Amundsen Sea. *Geophysical Research Letters*, *49*(24). doi: 10.1029/2022gl100646

Spence, P., Griffies, S. M., England, M. H., Hogg, A. M., Saenko, O. A., & Jourdain, N. C. (2014, jul). Rapid subsurface warming and circulation changes of Antarctic coastal waters by poleward shifting winds. *Geophysical Research Letters*, *41*(13), 4601–4610. doi: 10.1002/2014gl060613

Steig, E., Ding, Q., Battisti, D., & Jenkins, A. (2012). Tropical forcing of Circumpolar Deep Water Inflow and outlet glacier thinning in the Amundsen Sea Embayment, West Antarctica. *Annals of Glaciology*, *53*(60), 19–28. doi:

10.3189/2012aog60a110

Stewart, A. L., Klocker, A., & Menemenlis, D. (2019, aug). Acceleration and Overturning of the Antarctic Slope Current by Winds, Eddies, and Tides. *Journal of Physical Oceanography*, *49*(8), 2043–2074. doi: 10.1175/jpo-d-18-0221.1

Thoma, M., Jenkins, A., Holland, D., & Jacobs, S. (2008, sep). Modelling Circumpolar Deep Water intrusions on the Amundsen Sea continental shelf, Antarctica. *Geophysical Research Letters*, *35*(18). doi: 10.1029/2008gl034939

Walker, D. P., Brandon, M. A., Jenkins, A., Allen, J. T., Dowdeswell, J. A., & Evans, J. (2007, jan). Oceanic heat transport onto the Amundsen Sea shelf through a submarine glacial trough. *Geophysical Research Letters*, *34*(2). doi: 10.1029/2006gl028154

Walker, D. P., Jenkins, A., Assmann, K. M., Shoosmith, D. R., & Brandon, M. A. (2013, jun). Oceanographic observations at the shelf break of the Amundsen Sea, Antarctica. *Journal of Geophysical Research: Oceans*, *118*(6), 2906–2918. doi: 10.1002/jgrc.20212

Webber, B. G. M., Heywood, K. J., Stevens, D. P., & Assmann, K. M. (2019, jan). The Impact of Overturning and Horizontal Circulation in Pine Island Trough on Ice Shelf Melt in the Eastern Amundsen Sea. *Journal of Physical Oceanography*, *49*(1), 63–83. doi: 10.1175/jpo-d-17-0213.1

Wåhlin, A. K., Kalén, O., Arneborg, L., Björk, G., Carvajal, G. K., Ha, H. K., ... Stranne, C. (2013, October). Variability of Warm Deep Water Inflow in a Submarine Trough on the Amundsen Sea Shelf. *Journal of Physical Oceanography*, *43*(10), 2054–2070. doi: 10.1175/jpo-d-12-0157.1

Decadal variability of ice-shelf melting in the Amundsen Sea driven by sea-ice freshwater fluxes

Michael Haigh[1] and Paul R. Holland[1]

[1]British Antarctic Survey, Cambridge, UK

Key Points:

- An undercurrent flowing along the Amundsen Sea shelf break regulates oceanic ice-shelf melting in the region.
- Model results have shown that decadal variability of the undercurrent opposes the wind variability.
- We show that sea-ice freshwater flux anomalies linked to tropical Pacific variability regulate the undercurrent and ice-shelf melting.

Corresponding author: Michael Haigh, `michai@bas.ac.uk`

Abstract

The ice streams flowing into the Amundsen Sea, West Antarctica, are losing mass due to changes in the oceanic basal melting of their floating ice shelves. Rapid ice-shelf melting is sustained by the delivery of warm Circumpolar Deep Water to the ice-shelf cavities, which is first supplied to the continental shelf by an undercurrent that flows eastward along the shelf break. Temporal variability of this undercurrent controls ice-shelf basal melt variability. Recent work shows that on decadal timescales the undercurrent variability opposes surface wind variability. Using a regional model, we show that undercurrent variability is driven by sea-ice freshwater fluxes, particularly those north of the shelf break, which affect the cross-shelf break density gradient. This sea-ice variability is caused by tropical Pacific variability impacting atmospheric conditions over the Amundsen Sea. Ice-shelf melting also feeds back onto the undercurrent by affecting the on-shelf density, thereby influencing shelf-break density gradient anomalies.

Plain Language Summary

The glaciers that flow towards the Amundsen Sea, West Antarctica, are losing ice faster than most others about the continent. Once these glaciers reach the coast, they extend out onto the ocean surface, forming ice shelves. The rapid loss of ice is caused by changes in melting by relatively warm ocean waters beneath the floating ice shelves. In the Amundsen Sea, a deep ocean current is responsible for delivering warm water from the deep ocean to the ice shelves. We present model results that show that this deep current varies on decadal timescales as a consequence of systematic sea-ice melt and formation patterns. A faster current drives more rapid ice shelf melting which, via a feedback process, further accelerates the current. Climate variability originating in the tropical Pacific Ocean is responsible for the variability in the sea-ice, and is therefore also responsible for the effects on melting of the ice shelves.

1 Introduction

Melting of the West Antarctic Ice Sheet provides Antarctica's biggest contribution to global sea-level rise (Shepherd et al., 2018), with the ice streams draining into the Amundsen Sea of particular concern (Mouginot et al., 2014; Rignot et al., 2014; Joughin et al., 2014). Rapid ice loss in this region is due to the access of warm Circumpolar Deep Water (CDW) to the undersides of the ice shelves, the floating extensions of the grounded ice streams (Jacobs et al., 1996; Dutrieux et al., 2014; Heywood et al., 2016). Ocean modelling studies suggest that this basal melting increased over the 20th century due to anthropogenic forcing (Naughten et al., 2022), and will continue to increase during the 21st century (Jourdain et al., 2022; Naughten et al., 2023). Superimposed on any such long-term trends are the impacts of strong natural decadal climate variability (Dutrieux et al., 2014; Jenkins et al., 2018), on which we focus in this study.

Access of CDW to the Amundsen Sea ice shelves is controlled by an undercurrent that flows along the continental shelf break. As observed (Walker et al., 2007, 2013; Assmann et al., 2013) and modelled (Thoma et al., 2008; Kimura et al., 2017; Webber et al., 2019; Caillet et al., 2022), the undercurrent flows eastward along the shelf break, and is diverted onto the continental shelf by bathymetric troughs intersecting the shelf break. Through this process the undercurrent transports warm CDW onto the continental shelf, which then flows across the shelf and beneath the ice shelves. Changes in the undercurrent control the variability of ice-shelf melting (Jenkins et al., 2016; Dotto et al., 2019, 2020) and are implicated in historical and future changes in melting (Naughten et al., 2022, 2023). Therefore, understanding drivers of undercurrent variability is essential for understanding future melt of the vulnerable ice streams in the Amundsen Sea region.

The undercurrent exists due to the Antarctic Slope Front (ASF), which separates CDW north of the shelf break from the lighter, cooler and fresher waters to the south (Jacobs, 1991; Stewart et al., 2019). This creates a south-to-north pressure gradient which causes the flow to be more eastward with depth. Variability in the ASF, or wider ocean density variability, will drive baroclinic (depth-dependent) variability in the undercurrent. The density structure across the shelf break can be affected by a number of processes, including wind-driven downwelling/upwelling (Spence et al., 2014), surface buoyancy fluxes (Caillet et al., 2022), and ice-shelf basal melting (Moorman et al., 2020; Si et al., 2023).

Winds drive barotropic (depth-independent) variability in the undercurrent by influencing gradients in sea-surface height, such that eastward wind anomalies drive an eastward acceleration in both the surface and deep flow (Assmann et al., 2013; Jenkins et al., 2016; Dotto et al., 2019, 2020). This is thought to be the dominant mechanism on short (synoptic to interannual) timescales (Wåhlin et al., 2013; Silvano et al., 2022). However, the Amundsen Sea is impacted slower natural and anthropogenic climate changes that vary on interannual, interdecadal, and centennial timescales (Steig et al., 2012; Li et al., 2021; Holland et al., 2019, 2022). Recently, Silvano et al. (2022) presented regional model output showing that undercurrent variability actually opposes surface wind variability on decadal timescales, such that eastward (westward) shelf-break wind anomalies coincide with a weaker (stronger) eastward undercurrent, while the surface flow variability simply follows the winds. Silvano et al. (2022) hypothesised that this was due to wind-driven upwelling/downwelling anomalies on the continental shelf driving slow baroclinic variability that outweighs the faster barotropic effects of the shelf-break winds. In this study we examine the same regional model and demonstrate that this decadal baroclinic variability is in fact driven by sea-ice and ice-shelf freshwater fluxes.

2 Methods

2.1 Amundsen Sea regional model

Following Silvano et al. (2022), we use the Massachusetts Institute of Technology general circulation model (MITgcm) including ocean, sea-ice and ice-shelf components, with the same configuration as Naughten et al. (2022) with one minor difference in the application of iceberg meltwater. The model domain spans the longitudes 140°W to 80°W and latitudes 75.5°S to 62°S. The lateral grid resolution is 0.1° in longitude, corresponding to an isotropic grid spacing of ~ 2.75 km in the south and ~ 5.15 km in the north. The vertical direction is discretised by 50 levels with the thinnest (10 m) levels near the surface and the thickest (200 m) levels near the ocean bottom. The model is forced by six-hourly ERA5 (Hersbach et al., 2020) 10 m winds, surface longwave and shortwave radiation, 2 m air temperature, 2 m specific humidity, precipitation and atmospheric pressure. The model is spun up using the 1979-2002 interval of the external forcing data. After this spinup, the forcing is restarted from 1979 and the model is run until 2019 with monthly mean output. Our analysis is based on model output during 1984-2019. Further details of the model can be found in Naughten et al. (2022).

2.2 Definition of the undercurrent

The eastward undercurrent is defined using an approach very similar to Silvano et al. (2022). We start by locating the 1000 m isobath at the shelf break between 125°W and 108°W, the undercurrent longitudes of interest. For each longitude along the isobath, the along-slope flow beneath the 1028 kg m^{-3} isopycnal and above 800 m depth is averaged over a meridional range of three grid points either side of the isobath. The undercurrent speed is then defined as the maximum of these meridionally averaged values at any depth, which typically occurs near 500 m depth. The along-slope surface current and winds are computed at each longitude as an average over the same meridional range. All quantities are then averaged along the undercurrent pathway, with the Dotson-Getz and Pine Island-Thwaites West troughs excluded from the computations. Similar to Silvano et al. (2022), we find that using alternate undercurrent definitions does not affect our conclusions.

2.3 Statistical methods

We use a combination of correlations and composites to analyse model output. For correlations we use the Pearson correlation coefficient r and significance p, the latter computed using a two-sided Student's t-test. When computing the significance we account for the effective degrees of freedom, defined as the number of time samples divided by twice the e-folding decorrelation timescale. Doing this is important since we focus on decadal variability, but have model output spanning only a few decades. For the same reason, not all provided correlations are significant at the 95% level. Significance values will be provided with each correlation coefficient.

For composites of a response field against a scalar predictor, the positive (negative) composite is computed by averaging anomalies of the response field over all months for which the predictor is half a standard deviation greater (less) than its mean. We use two predictors: the undercurrent speed timeseries described above, and the Tripole Index (TPI) of the Interdecadal Pacific Oscillation (IPO).

We use the TPI as a means to quantify the influence of tropical Pacific variability, which dominates variability in the Amundsen Sea (Steig et al., 2012; Dutrieux et al., 2014; Li et al., 2021). Previous studies have separated this variability into two modes: El Niño-Southern Oscillation (ENSO) on shorter timescales and the IPO on longer (>13-year) timescales (Newman et al., 2016; Li et al., 2021). The monthly TPI is designed to quantify the longer IPO variability (Henley et al., 2015), but is also highly correlated to all ENSO indices (Holland et al., 2019). Since the timescale under consideration here is intermediate between ENSO and IPO, we use the monthly TPI index to represent all Pacific variability, without ascribing the variability to either mode. In this study, this index and all other timeseries are detrended, deseasoned and have a 5-year running mean applied. The only exception is in section 3.3, where we consider tropical Pacific impacts on wintertime atmospheric fields over the Amundsen Sea.

3 Results

3.1 The Amundsen Sea undercurrent

Fig. 1a shows the time-mean (1984-2019) flow and potential temperature at 455 m depth in the Amundsen Sea. Consistent with observations (Walker et al., 2007, 2013), the eastward undercurrent follows the continental slope and is guided southwards onto the shelf by bathymetric troughs at the shelf break. Through this process, warm CDW is advected onto the continental shelf, and eventually towards the ice shelves.

Fig. 1b shows timeseries of the along-slope undercurrent, surface current, surface winds and the ice-shelf basal melt integrated over all the ice shelves shown in Fig. 1a. Getz Ice Shelf west of 125°W is omitted from this computation since this part of its cavity is not supplied with CDW by the undercurrent. As first reported by Silvano et al. (2022), on decadal timescales the undercurrent is anticorrelated with the surface current ($r = -0.62$, $p = 0.09$) and weakly anticorrelated with the winds ($r = -0.26$, $p = 0.48$). The role of the undercurrent in controlling the ice-shelf basal melt is reflected in the strong positive correlation ($r = 0.96$, $p < 0.05$) between these two timeseries.

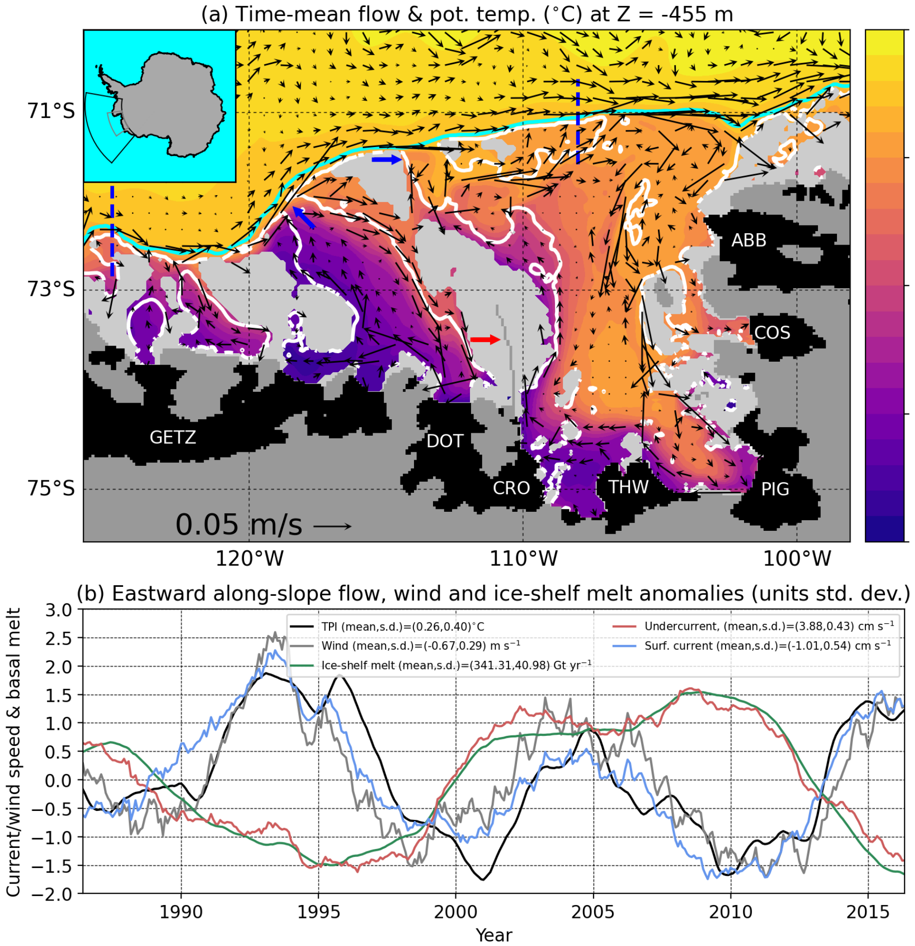

Figure 1. (a) Time-mean (1984-2019) flow (arrows, every six grid points) and potential temperature (colour, °C) at 455 m depth from model output. The cyan (white) contour represents the 1000 m (500 m) isobath. Light grey masking represents bathymetry shallower than 455 m, dark grey masking represents land and black masking represents the ice shelves (GETZ=Getz, DOT=Dotson, CRO=Crosson, THW=Thwaites, PIG=Pine Island Glacier, COS=Cosgrove, ABB=Abbot). Blue arrows indicate the Dotson-Getz and Pine Island-Thwaites West troughs. The red arrow indicates Bear Ridge, on which grounded icebergs sit (Bett et al., 2020). Inset: map showing model domain (black box) and subregion shown in this figure (grey box). (b) Timeseries of along-slope undercurrent, surface current, winds, area-integrated ice-shelf basal melt and TPI. Timeseries are demeaned and normalised by their standard deviations (see legend).

3.2 Density anomalies and freshwater fluxes

Fig. 2a shows the time-mean cross-slope density and along-slope velocity averaged along the undercurrent pathway, with y-coordinate centered on the 1000 m isobath. The southward deepening of density contours over the shelf break represents the ASF. Although the ASF is typically weaker in the Amundsen Sea compared to other sectors about Antarctica, it is nonetheless strong enough for the time-mean flow to transition from weak westward flow near the surface to strong eastward (~ 5 cm s^{-1}) flow at 300–500 m depth.

Figs. 2c,e show composites using the undercurrent speed as the predictor and the along-slope velocity and cross-slope density as the response fields. Eastward undercurrent anomalies coincide with negative density anomalies on the continental shelf that span most of the water column, and positive density anomalies north of the shelf break concentrated in the top 50 m of the water column. Density anomalies with the same spatial distribution but opposite sign are diagnosed for westward undercurrent anomalies. Cross-slope pressure gradient anomalies (not shown) very closely resemble undercurrent anomalies, confirming that the undercurrent decadal variability is both geostrophic and caused by these density anomalies.

We now consider winds and freshwater fluxes, both potential drivers of the density and undercurrent variability. Fig. 2b shows the time-mean winds, sea-ice freshwater flux (positive values freshen the ocean), and ice-shelf freshwater flux. Fig. 2d,f shows composites of the freshwater flux and wind responses to the undercurrent speed predictor. The wind composites can be used to test the hypothesis of Silvano et al. (2022), i.e., that anomalous wind-driven upwelling/downwelling on the continental shelf drives the undercurrent variability. Coastal wind anomalies tend to be weak and, importantly, are not oriented in the direction required to support this hypothesis. For example, during eastward undercurrent anomalies, coastal wind anomalies are predominantly eastward and induce coastal upwelling anomalies which would weaken, rather than strengthen, the shelf-break baroclinicity/undercurrent. Composites of the wind stress curl anomaly response to the undercurrent predictor (Fig. S1) also suggest that wind-driven upwelling/downwelling does not drive the undercurrent variability. Therefore, with the conclusion that wind-driven effects are not responsible for the decadal variability, we move on to consider freshwater fluxes.

The composites in Fig. 2d,f illustrate how freshwater flux anomalies drive the density and undercurrent variability (Fig. 2c,e). North of the shelf break, relatively dense (light) surface waters that contribute to eastward (westward) undercurrent anomalies are a result of anomalous sea-ice-driven salinification (freshening). The on-shelf density anomalies, which have sign opposite to those off-shelf, are predominantly due to ice-shelf freshwater flux variability. We propose that this ice-shelf melt variability is initially a response to the undercurrent variability driven by sea-ice freshwater fluxes. Then a positive feedback between the undercurrent and ice-shelf melting is initiated, whereby ice-shelf meltwater anomalies impact the on-shelf density and shelf-break density gradient, reinforcing undercurrent anomalies. Over time, the on-shelf density anomalies extrude off of the continental shelf, leading to a reduction the in cross-shelf density gradient anomalies that had previously built up.

During eastward undercurrent anomalies, on-shelf sea-ice freshwater flux anomalies (Fig. 2d) have opposite sign to those off-shelf, especially in coastal areas and near Bear Ridge (red arrow, Fig 1a), further contributing to the cross-slope density gradient anomaly. During westward undercurrent anomalies, however, on-shelf sea-ice freshwater flux anomalies (Fig. 2f) do not have a distinct spatial pattern.

More evidence of the mechanism by which freshwater fluxes drive undercurrent variability is provided by idealised modelling results (Figs. S2 and S3) using the MITgcm configuration of Haigh et al. (2023). In these simulations, decadally varying surface fresh-

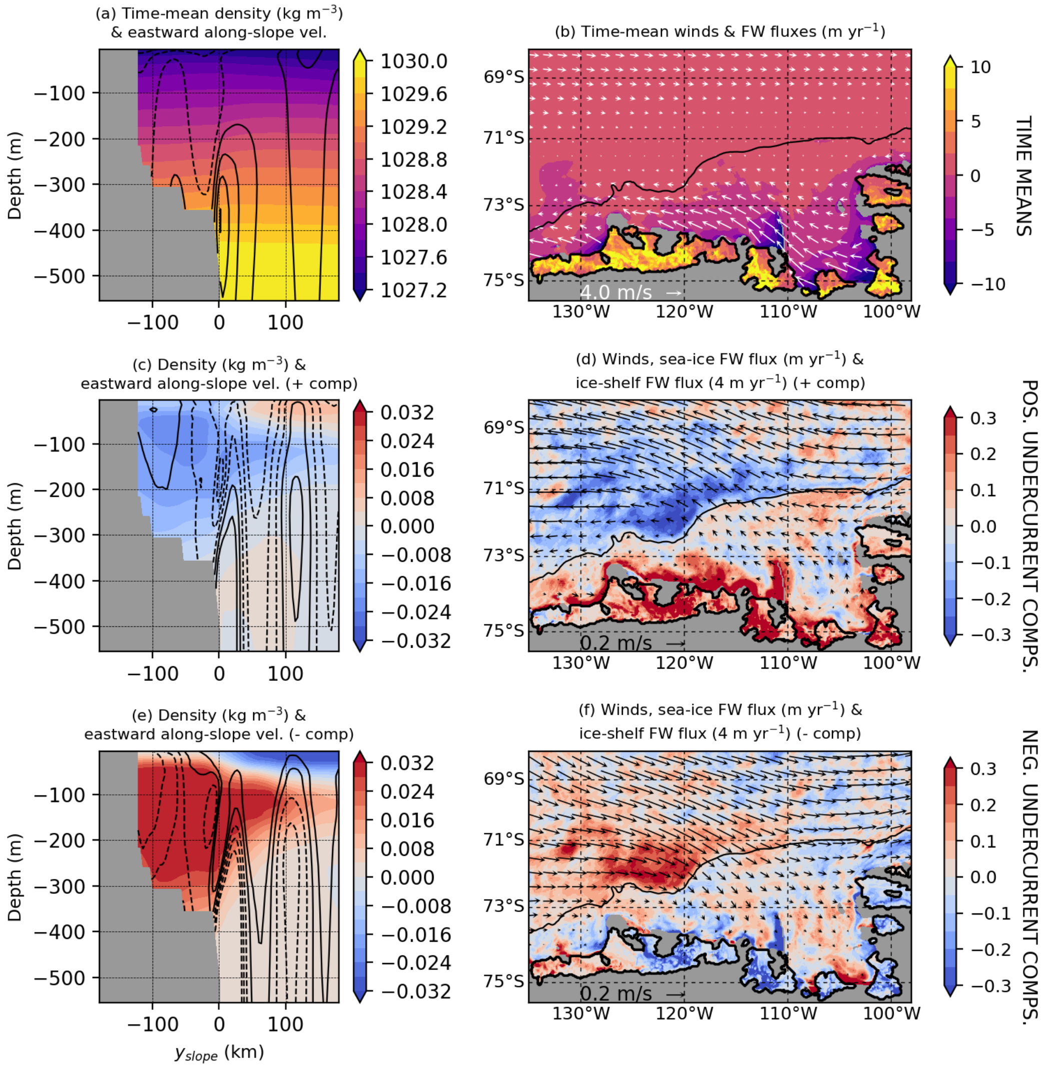

Figure 2. (a) Time-mean density (colour, kg m^{-3}) and eastward along-slope velocity (contours, 1 cm s^{-1} contour interval, dashed are zero and negative) averaged along the undercurrent pathway. (b) Time-mean winds (arrows) and sea-ice and ice-shelf freshwater fluxes (colour, m yr^{-1}). (c,e) Composites of density and eastward along-slope velocity (1 mm s^{-1} contour interval) for eastward/westward undercurrent anomalies. (d,f) Composites of sea-ice freshwater fluxes (m yr^{-1}), ice-shelf freshwater fluxes (4 m yr^{-1}) and winds for eastward/westward undercurrent anomalies. In (b,d,f) the thick black contour outlines the ice-shelf drafts and the thin black contour is the 1000 m shelf-break isobath.

water fluxes are applied and are shown to drive a decadally varying undercurrent by impacting the cross-shelf break density gradient.

Fig. 3a shows a correlation map with the undercurrent strength as predictor and sea-ice and ice-shelf freshwater fluxes as response fields, further quantifying the mechanism by which freshwater fluxes drive decadal variability in the undercurrent. The undercurrent negatively correlates ($r \approx 0.8$, $p < 0.05$) with sea-ice freshening anomalies north of the shelf break, but not those downstream of the undercurrent longitudes (east of 108°W). The undercurrent positively correlates (not significant) with sea-ice freshening anomalies over most of the continental shelf, in particular near Bear Ridge and in front of Getz ice shelf. Strong positive correlations ($r \approx 0.9$, $p < 0.05$) between the undercurrent and ice-shelf basal melt are suggestive of the feedback mechanism that exists between the two.

Fig. 3b shows timeseries of the sea-ice freshwater flux anomalies, integrated over the on-shelf and off-shelf regions shown in Fig. 3a. These regions are selected such that they span the same longitudes and have the same area. Also shown in Fig 3b are timeseries of the difference between the on-shelf and off-shelf freshwater flux anomalies, and the area-integrated ice-shelf freshwater flux anomaly. We exclude the western half of Getz Ice Shelf from the latter integral since it is not supplied with CDW by the undercurrent, although its meltwater may still impact the undercurrent. These timeseries are not sensitive to the precise choice of the areas of integration. The negation of the off-shelf flux anomaly is shown so that, for all timeseries, positive values correspond to an eastward acceleration of the undercurrent.

Apparently by coincidence, area-integrated ice-shelf and sea-ice freshwater flux anomalies have a very similar magnitude (Bett et al., 2020), suggesting that they make similar contributions to the undercurrent decadal variability. The undercurrent negatively correlates with the off-shelf sea-ice freshwater flux ($r = -0.69$, $p < 0.05$), does not notably correlate with the on-shelf sea-ice freshwater flux ($r = 0.20$, $p = 0.62$), but does notably correlate with their difference ($r = 0.71$, $p = 0.08$). These correlations reflect how the integrated off-shelf sea-ice freshwater flux has a distinct decadal variability similar to the undercurrent, whereas the on-shelf sea-ice freshwater flux does not (Fig 3b).

3.3 The role of tropical Pacific variability

While decadal variability in the ice-shelf basal melt is attributed to the undercurrent, the driver of decadal variability in the sea-ice freshwater fluxes remains to be determined. Here we attribute sea-ice freshwater flux variability to tropical Pacific variability, as quantified by the TPI (section 2.3). Positive (negative) phases of ENSO and the IPO are typically associated with a filled (deepened) Amundsen Sea Low (ASL) (Lachlan-Cope & Connolley, 2006; Clem et al., 2019; Li et al., 2021). This corresponds to eastward (westward) wind anomalies at the shelf break, which explains the decadal variability of the along-shelf break surface flow (Silvano et al., 2022) and its correlation with the TPI ($r = 0.91$, $p < 0.05$; Fig. 1b).

The negative correlation between the undercurrent and the TPI ($r = -0.63$, $p = 0.07$; Fig. 1b) is found to be caused by the impacts of Pacific variability on atmospheric conditions over the Amundsen Sea during austral winter (JJA), the season during which tropical teleconnections with the region are strongest (Ding et al., 2011; Li et al., 2021). Fig. 4a,b shows composites of the winter sea-ice freshwater flux anomaly during positive and negative phases of the TPI. Similar to the relationship between freshwater fluxes and undercurrent speed (Figs. 2 and 3), there is anomalous sea-ice-driven freshening (salinification) north of the shelf break during positive (negative) composites of the TPI. The spatial distribution of the on-shelf sea-ice freshwater flux anomaly is less distinct, and its sign tends to follow the anomaly north of the shelf break.

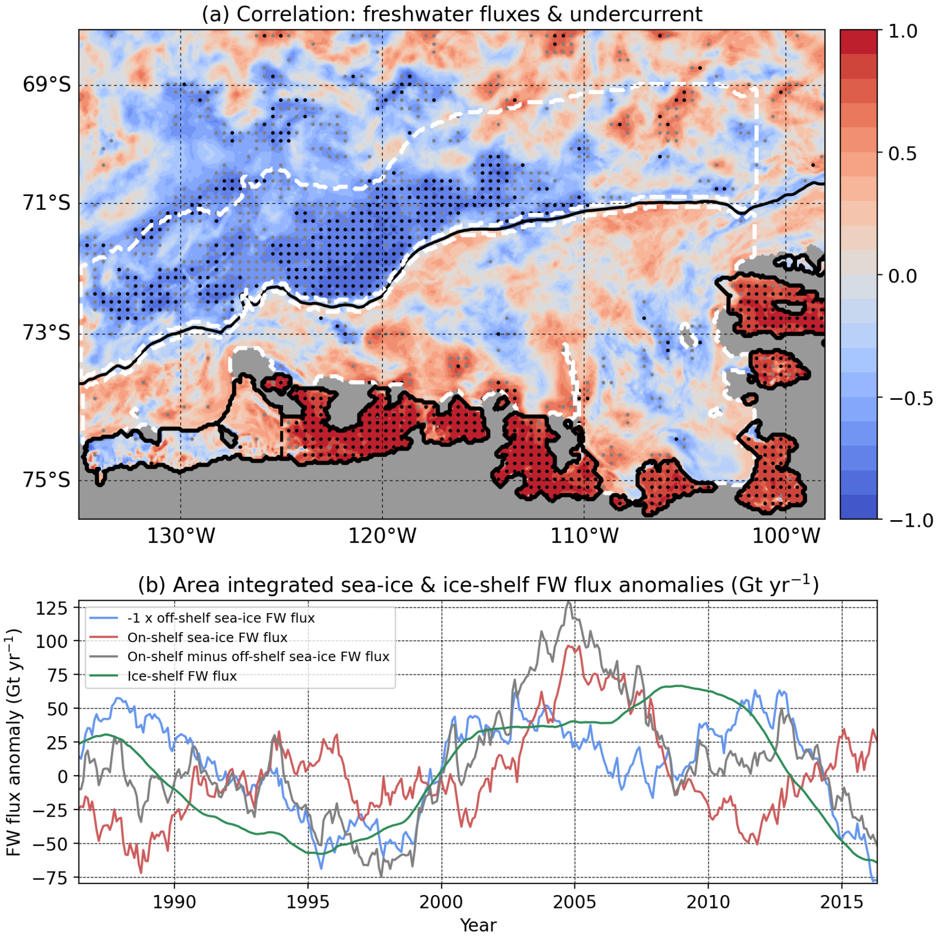

Figure 3. (a) Correlation between the undercurrent speed and the sea-ice and ice-shelf freshwater fluxes into the ocean. Black (grey) stippling denotes significance $p < 0.05$ ($p < 0.15$). The thick black contour outlines the ice-shelf drafts and the thin black contour is the 1000 m shelf-break isobath. (b) Timeseries of area-integrated freshwater flux anomalies (Gt yr^{-1}), oriented such that positive values strengthen the undercurrent. Plotted are the on-shelf sea-ice freshwater flux anomaly (red), the negation of the off-shelf sea-ice freshwater flux anomaly (blue), the on-shelf minus off-shelf sea-ice freshwater fluxes (grey) and the ice-shelf freshwater flux anomaly (green). Areas of integration for the sea-ice freshwater fluxes are outlined by the white contours in panel (a). The ice-shelf freshwater flux is integrated over all ice shelves shown in panel (a), excluding the area of the Getz Ice Shelf west of 125°W.

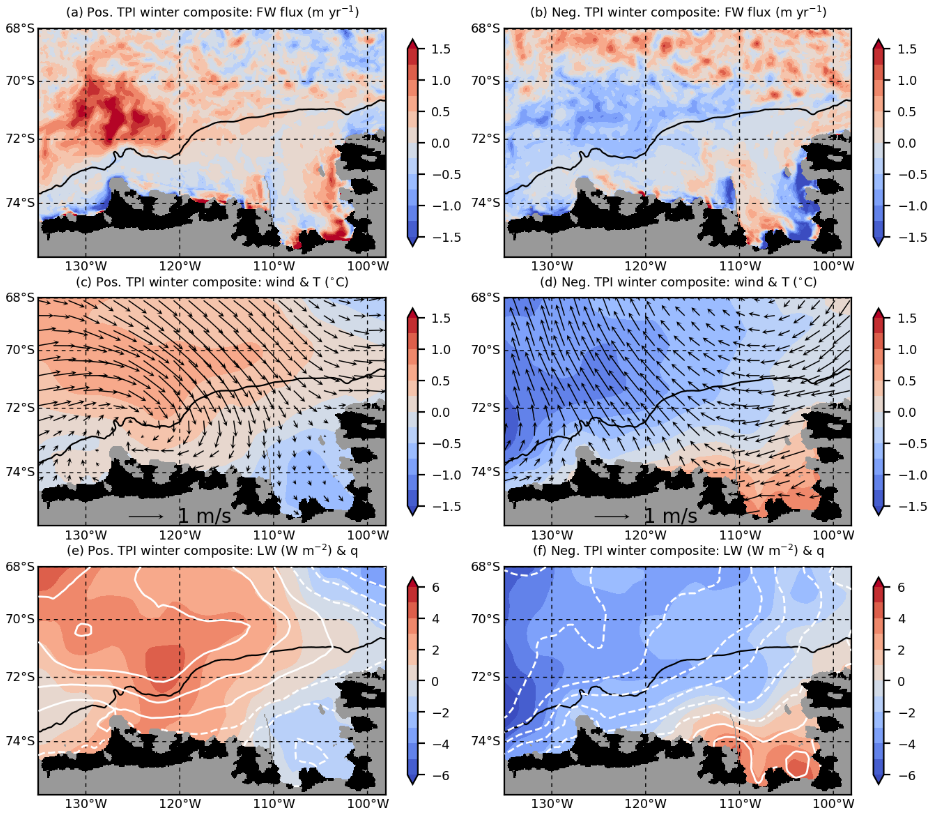

Figure 4. Winter (JJA) composites using the TPI as the predictor and freshwater fluxes and atmospheric conditions as the response fields. (a,b) Composites of the winter sea-ice freshwater flux anomaly (m yr^{-1}) during positive/negative TPI. (c,d) Composites of the winter 10 m wind (arrows) and 2 m air temperature, T (colour, °C) during positive/negative TPI. (e,f) Composites of the winter downward longwave radiation (colour, W m^{-2}) and 2 m specific humidity, q (white contours, 2.5×10^{-5} kg kg^{-1} contour interval, dashed are zero and negative) during positive/negative TPI.

Figs. 4c,d show composites of the ERA5 10 m winds and 2 m air temperature responses to the TPI predictor, and Figs. 4e,f show composites of the downward longwave (LW) radiation and 2 m specific humidity responses. During positive phases of the TPI, the weakened ASL creates northerly wind anomalies over the deep ocean. This transports relatively warm and moist air southwards over the region north of the shelf break, leading to greater downward LW radiation. As such, during positive phases of the TPI, all of the wintertime sea-ice surface heat fluxes (sensible and latent heat fluxes and LW radiation) are anomalously downwards, leading to a reduction in sea-ice formation and even periods of absolute sea-ice melt north of the shelf break. During negative phases of the TPI the opposite process occurs, causing greater sea-ice formation north of the shelf break.

For a given phase of the TPI, anomalies in thermodynamic atmospheric fields on the continental shelf have the opposite sign to anomalies north of the shelf break. However, freshwater flux anomalies on the continental shelf tend to have the same sign as anomalies north of the shelf break. This behaviour can be explained by winds near the coast: during negative phases of the TPI, wind anomalies tend to be directed away from the coast, opening coastal polynyas, forming more sea ice and driving greater brine rejection. During positive TPI phases, the opposite process occurs, although the coastal wind anomalies are weaker. The contrasting effects of coastal winds and thermodynamic atmospheric anomalies cause the indistinct spatial distribution of the on-shelf sea-ice freshwater fluxes and also cause the lack of distinct decadal variability compared to the off-shelf fluxes (Fig. 3b). These contrasting effects are also reflected by the weak correlation between the TPI and the on-shelf sea-ice freshwater fluxes ($r = 0.33$, $p = 0.39$) relative to the correlation between the TPI and the off-shelf fluxes ($r = 0.53$, $p = 0.15$).

4 Discussion and Conclusions

Understanding the variability of the Amundsen Sea eastward undercurrent is of great importance since it modulates basal melting of the ice shelves in the region. Until recently the undercurrent was thought to simply vary with the winds over the continental shelf break. However, Silvano et al. (2022) recently presented model results showing that on decadal timescales the undercurrent variability actually opposes wind variability. In this study we show that this undercurrent decadal variability is driven by a combination of sea-ice and ice-shelf freshwater fluxes.

Composites of our regional model output show that on decadal timescales eastward (westward) undercurrent anomalies are due to anomalous sea-ice-driven salinification (freshening) north of the shelf break which enhances (weakens) the cross-slope baroclinicity. Decadal variability in the sea-ice freshwater flux is due to tropical Pacific variability and its impact on the ASL during winter (Lachlan-Cope & Connolley, 2006; Clem et al., 2019; Li et al., 2021). During positive (negative) phases of the TPI, northerly (southerly) wind anomalies transport relatively warm and moist (cold and dry) air to the area north of the shelf break. The associated downward (upward) heat flux anomalies drive the diagnosed sea-ice freshening (salinification) anomalies. Periods of faster (slower) undercurrent lead to enhanced (reduced) ice-shelf basal melt. These ice-shelf basal melt anomalies create on-shelf density anomalies which reinforce the anomalies in the cross-slope pressure gradient (Moorman et al., 2020; Si et al., 2023) and undercurrent.

Our results are consistent with the simulations of Caillet et al. (2022), who perturb precipitation and air temperature over the Amundsen Sea continental shelf. These perturbations lead to surface buoyancy flux anomalies which impact the on-shelf density and induce undercurrent anomalies via the same mechanism as in this study. While Caillet et al. (2022) discussed buoyancy fluxes on the continental shelf, our results show that fluxes over the deep ocean are important for the Amundsen Sea undercurrent and ice shelves.

The conclusions of our study are based on one regional model simulation spanning just two periods of the decadal variability. For this reason presented timeseries have few effective degrees of freedom, meaning some provided correlations are not significant at the 95% level. For example, while the correlation between the undercurrent and off-shelf sea-ice freshwater flux is significant ($r = -0.69$, $p < 0.05$), the correlation between the TPI and the off-shelf fluxes ($r = 0.53$, $p = 0.15$) is not. Therefore, there is confidence in the link between the freshwater fluxes and the undercurrent, but further modelling efforts are necessary to gain more confidence in the link to tropical Pacific variability.

In this study we have focussed on natural decadal variability. However, the Amundsen Sea region is impacted by anthropogenic effects, driving trends in the regional winds (Goyal et al., 2021; Holland et al., 2022) which can drive trends in ocean conditions, in particular increasing the on-shelf heat content (Spence et al., 2014; Naughten et al., 2022). Climate projections show that ice-shelf basal melt in the Amundsen Sea is expected to increase over the next century (Jourdain et al., 2022; Naughten et al., 2023), a trend on which the decadal variability considered here is superimposed. Improving our understanding of both the anthropogenic trends and the natural variability remains a crucial challenge which must be tackled for society to mitigate against and adapt to future sea-level rise.

Data Availability Statement

The data and post-processing codes used in this study are available for download from Haigh and Holland (2024). Data for the Tripole Index (Henley et al., 2015) for the Interdecadal Pacific Oscillation can be found at https://psl.noaa.gov/data/timeseries/IPOTPI/.

Acknowledgments

This research was funded by the NERC project "Drivers of Oceanic Change in the Amundsen Sea", NE/T012803/1.

References

Assmann, K. M., Jenkins, A., Shoosmith, D. R., Walker, D. P., Jacobs, S. S., & Nicholls, K. W. (2013, dec). Variability of Circumpolar Deep Water transport onto the Amundsen Sea Continental shelf through a shelf break trough. *Journal of Geophysical Research: Oceans*, *118*(12), 6603–6620. doi: 10.1002/2013jc008871

Bett, D. T., Holland, P. R., Garabato, A. C. N., Jenkins, A., Dutrieux, P., Kimura, S., & Fleming, A. (2020, sep). The Impact of the Amundsen Sea Freshwater Balance on Ocean Melting of the West Antarctic Ice Sheet. *Journal of Geophysical Research: Oceans*, *125*(9). doi: 10.1029/2020jc016305

Caillet, J., Jourdain, N. C., Mathiot, P., Hellmer, H. H., & Mouginot, J. (2022, December). Drivers and Reversibility of Abrupt Ocean State Transitions in the Amundsen Sea, Antarctica. *Journal of Geophysical Research: Oceans*, *128*(1). doi: 10.1029/2022jc018929

Clem, K. R., Lintner, B. R., Broccoli, A. J., & Miller, J. R. (2019, June). Role of the South Pacific Convergence Zone in West Antarctic Decadal Climate Variability. *Geophysical Research Letters*, *46*(12), 6900–6909. doi: 10.1029/2019gl082108

Ding, Q., Steig, E. J., Battisti, D. S., & Küttel, M. (2011, April). Winter warming in West Antarctica caused by central tropical Pacific warming. *Nature Geoscience*, *4*(6), 398–403. doi: 10.1038/ngeo1129

Dotto, T. S., Garabato, A. C. N., Bacon, S., Holland, P. R., Kimura, S., Firing, Y. L., ... Jenkins, A. (2019, nov). Wind-Driven Processes Controlling Oceanic

Heat Delivery to the Amundsen Sea, Antarctica. *Journal of Physical Oceanography*, *49*(11), 2829–2849. doi: 10.1175/jpo-d-19-0064.1

Dotto, T. S., Garabato, A. C. N., Wåhlin, A. K., Bacon, S., Holland, P. R., Kimura, S., . . . Jenkins, A. (2020, aug). Control of the Oceanic Heat Content of the Getz-Dotson Trough, Antarctica, by the Amundsen Sea Low. *Journal of Geophysical Research: Oceans*, *125*(8). doi: 10.1029/2020jc016113

Dutrieux, P., Rydt, J. D., Jenkins, A., Holland, P. R., Ha, H. K., Lee, S. H., . . . Schröder, M. (2014, jan). Strong Sensitivity of Pine Island Ice-Shelf Melting to Climatic Variability. *Science*, *343*(6167), 174–178. doi: 10.1126/science.1244341

Goyal, R., Gupta, A. S., Jucker, M., & England, M. H. (2021, feb). Historical and Projected Changes in the Southern Hemisphere Surface Westerlies. *Geophysical Research Letters*, *48*(4). doi: 10.1029/2020gl090849

Haigh, M., & Holland, P. R. (2024). *Data for Decadal variability of ice-shelf melt in the Amundsen Sea driven by freshwater fluxes.* Zenodo. doi: 10.5281/ZENODO.10391364

Haigh, M., Holland, P. R., & Jenkins, A. (2023, May). The Influence of Bathymetry Over Heat Transport Onto the Amundsen Sea Continental Shelf. *Journal of Geophysical Research: Oceans*, *128*(5). doi: 10.1029/2022jc019460

Henley, B. J., Gergis, J., Karoly, D. J., Power, S., Kennedy, J., & Folland, C. K. (2015, March). A Tripole Index for the Interdecadal Pacific Oscillation. *Climate Dynamics*, *45*(11–12), 3077–3090. doi: 10.1007/s00382-015-2525-1

Hersbach, H., Bell, B., Berrisford, P., Hirahara, S., Horányi, A., Muñoz-Sabater, J., . . . Thépaut, J. (2020, June). The ERA5 global reanalysis. *Quarterly Journal of the Royal Meteorological Society*, *146*(730), 1999–2049. doi: 10.1002/qj.3803

Heywood, K., Biddle, L., Boehme, L., Dutrieux, P., Fedak, M., Jenkins, A., . . . Webber, B. (2016, dec). Between the Devil and the Deep Blue Sea: The Role of the Amundsen Sea Continental Shelf in Exchanges Between Ocean and Ice Shelves. *Oceanography*, *29*(4), 118–129. doi: 10.5670/oceanog.2016.104

Holland, P. R., Bracegirdle, T. J., Dutrieux, P., Jenkins, A., & Steig, E. J. (2019, aug). West Antarctic ice loss influenced by internal climate variability and anthropogenic forcing. *Nature Geoscience*, *12*(9), 718–724. doi: 10.1038/s41561-019-0420-9

Holland, P. R., O'Connor, G. K., Bracegirdle, T. J., Dutrieux, P., Naughten, K. A., Steig, E. J., . . . Smith, J. A. (2022, December). Anthropogenic and internal drivers of wind changes over the Amundsen Sea, West Antarctica, during the 20th and 21st centuries. *The Cryosphere*, *16*(12), 5085–5105. doi: 10.5194/tc-16-5085-2022

Jacobs, S. S. (1991, nov). On the nature and significance of the Antarctic Slope Front. *Marine Chemistry*, *35*(1-4), 9–24. doi: 10.1016/s0304-4203(09)90005-6

Jacobs, S. S., Hellmer, H. H., & Jenkins, A. (1996, may). Antarctic Ice Sheet melting in the southeast Pacific. *Geophysical Research Letters*, *23*(9), 957–960. doi: 10.1029/96gl00723

Jenkins, A., Dutrieux, P., Jacobs, S., Steig, E., Gudmundsson, H., Smith, J., & Heywood, K. (2016, dec). Decadal Ocean Forcing and Antarctic Ice Sheet Response: Lessons from the Amundsen Sea. *Oceanography*, *29*(4), 106–117. doi: 10.5670/oceanog.2016.103

Jenkins, A., Shoosmith, D., Dutrieux, P., Jacobs, S., Kim, T. W., Lee, S. H., . . . Stammerjohn, S. (2018, aug). West Antarctic Ice Sheet retreat in the Amundsen Sea driven by decadal oceanic variability. *Nature Geoscience*, *11*(10), 733–738. doi: 10.1038/s41561-018-0207-4

Joughin, I., Smith, B. E., & Medley, B. (2014, may). Marine Ice Sheet Collapse Potentially Under Way for the Thwaites Glacier Basin, West Antarctica. *Science*, *344*(6185), 735–738. doi: 10.1126/science.1249055

Jourdain, N. C., Mathiot, P., Burgard, C., Caillet, J., & Kittel, C. (2022, November). Ice Shelf Basal Melt Rates in the Amundsen Sea at the End of the 21st Century. *Geophysical Research Letters*, *49*(22). doi: 10.1029/2022gl100629

Kimura, S., Jenkins, A., Regan, H., Holland, P. R., Assmann, K. M., Whitt, D. B., ... Dutrieux, P. (2017, dec). Oceanographic Controls on the Variability of Ice-Shelf Basal Melting and Circulation of Glacial Meltwater in the Amundsen Sea Embayment, Antarctica. *Journal of Geophysical Research: Oceans*, *122*(12), 10131–10155. doi: 10.1002/2017jc012926

Lachlan-Cope, T., & Connolley, W. (2006, December). Teleconnections between the tropical Pacific and the Amundsen-Bellinghausens Sea: Role of the El Niño/Southern Oscillation. *Journal of Geophysical Research: Atmospheres*, *111*(D23). doi: 10.1029/2005jd006386

Li, X., Cai, W., Meehl, G. A., Chen, D., Yuan, X., Raphael, M., ... Song, C. (2021, August). Tropical teleconnection impacts on Antarctic climate changes. *Nature Reviews Earth & Environment*, *2*(10), 680–698. doi: 10.1038/s43017-021-00204-5

Moorman, R., Morrison, A. K., & McC. Hogg, A. (2020, August). Thermal Responses to Antarctic Ice Shelf Melt in an Eddy-Rich Global Ocean–Sea Ice Model. *Journal of Climate*, *33*(15), 6599–6620. doi: 10.1175/jcli-d-19-0846.1

Mouginot, J., Rignot, E., & Scheuchl, B. (2014, mar). Sustained increase in ice discharge from the Amundsen Sea Embayment, West Antarctica, from 1973 to 2013. *Geophysical Research Letters*, *41*(5), 1576–1584. doi: 10.1002/2013gl059069

Naughten, K. A., Holland, P. R., & De Rydt, J. (2023, October). Unavoidable future increase in West Antarctic ice-shelf melting over the twenty-first century. *Nature Climate Change*, *13*(11), 1222–1228. doi: 10.1038/s41558-023-01818-x

Naughten, K. A., Holland, P. R., Dutrieux, P., Kimura, S., Bett, D. T., & Jenkins, A. (2022, mar). Simulated Twentieth-Century Ocean Warming in the Amundsen Sea, West Antarctica. *Geophysical Research Letters*, *49*(5). doi: 10.1029/2021gl094566

Newman, M., Alexander, M. A., Ault, T. R., Cobb, K. M., Deser, C., Di Lorenzo, E., ... Smith, C. A. (2016, June). The Pacific Decadal Oscillation, Revisited. *Journal of Climate*, *29*(12), 4399–4427. doi: 10.1175/jcli-d-15-0508.1

Rignot, E., Mouginot, J., Morlighem, M., Seroussi, H., & Scheuchl, B. (2014, may). Widespread, rapid grounding line retreat of Pine Island, Thwaites, Smith, and Kohler glaciers, West Antarctica, from 1992 to 2011. *Geophysical Research Letters*, *41*(10), 3502–3509. doi: 10.1002/2014gl060140

Shepherd, A., Ivins, E., Rignot, E., Smith, B., van den Broeke, M., Velicogna, I., ... others (2018, jun). Mass balance of the Antarctic Ice Sheet from 1992 to 2017. *Nature*, *558*(7709), 219–222. doi: 10.1038/s41586-018-0179-y

Si, Y., Stewart, A. L., & Eisenman, I. (2023, May). Heat transport across the Antarctic Slope Front controlled by cross-slope salinity gradients. *Science Advances*, *9*(18). doi: 10.1126/sciadv.add7049

Silvano, A., Holland, P. R., Naughten, K. A., Dragomir, O., Dutrieux, P., Jenkins, A., ... Naveira Garabato, A. C. (2022, December). Baroclinic Ocean Response to Climate Forcing Regulates Decadal Variability of Ice-Shelf Melting in the Amundsen Sea. *Geophysical Research Letters*, *49*(24). doi: 10.1029/2022gl100646

Spence, P., Griffies, S. M., England, M. H., Hogg, A. M., Saenko, O. A., & Jourdain, N. C. (2014, jul). Rapid subsurface warming and circulation changes of Antarctic coastal waters by poleward shifting winds. *Geophysical Research Letters*, *41*(13), 4601–4610. doi: 10.1002/2014gl060613

Steig, E., Ding, Q., Battisti, D., & Jenkins, A. (2012). Tropical forcing of Circumpolar Deep Water Inflow and outlet glacier thinning in the Amundsen Sea Embayment, West Antarctica. *Annals of Glaciology*, *53*(60), 19–28. doi:

10.3189/2012aog60a110

Stewart, A. L., Klocker, A., & Menemenlis, D. (2019, aug). Acceleration and Overturning of the Antarctic Slope Current by Winds, Eddies, and Tides. *Journal of Physical Oceanography*, *49*(8), 2043–2074. doi: 10.1175/jpo-d-18-0221.1

Thoma, M., Jenkins, A., Holland, D., & Jacobs, S. (2008, sep). Modelling Circumpolar Deep Water intrusions on the Amundsen Sea continental shelf, Antarctica. *Geophysical Research Letters*, *35*(18). doi: 10.1029/2008gl034939

Walker, D. P., Brandon, M. A., Jenkins, A., Allen, J. T., Dowdeswell, J. A., & Evans, J. (2007, jan). Oceanic heat transport onto the Amundsen Sea shelf through a submarine glacial trough. *Geophysical Research Letters*, *34*(2). doi: 10.1029/2006gl028154

Walker, D. P., Jenkins, A., Assmann, K. M., Shoosmith, D. R., & Brandon, M. A. (2013, jun). Oceanographic observations at the shelf break of the Amundsen Sea, Antarctica. *Journal of Geophysical Research: Oceans*, *118*(6), 2906–2918. doi: 10.1002/jgrc.20212

Webber, B. G. M., Heywood, K. J., Stevens, D. P., & Assmann, K. M. (2019, jan). The Impact of Overturning and Horizontal Circulation in Pine Island Trough on Ice Shelf Melt in the Eastern Amundsen Sea. *Journal of Physical Oceanography*, *49*(1), 63–83. doi: 10.1175/jpo-d-17-0213.1

Wåhlin, A. K., Kalén, O., Arneborg, L., Björk, G., Carvajal, G. K., Ha, H. K., ... Stranne, C. (2013, October). Variability of Warm Deep Water Inflow in a Submarine Trough on the Amundsen Sea Shelf. *Journal of Physical Oceanography*, *43*(10), 2054–2070. doi: 10.1175/jpo-d-12-0157.1

Supporting Information for "Decadal variability of ice-shelf melting in the Amundsen Sea driven by sea-ice freshwater fluxes"

Michael Haigh[1]& Paul R. Holland[1]

[1]British Antarctic Survey, Cambridge, UK

Contents of this file

Introduction

In this document we present additional output of the regional model used in this study. Fig. S1, which is discussed in Text S1, shows the time-mean and composites (using the undercurrent as the predictor) of the surface stress curl in the regional model. The data shown in this figure suggest that the surface stress curl is not responsible for driving the diagnosed decadal variability in the undercurrent and ice shelf melt.

We also present outputs of an idealised model used to reproduce the mechanism by which freshwater fluxes drive decadal variability of the Amundsen Sea undercurrent. The idealised model setup is shown in Fig. S2 and discussed in Text S2. The idealised model output is shown in Fig. S3 and discussed in Text S3.

Text S1

Silvano et al. (2022) presented model results showing that variability of the eastward undercurrent at the Amundsen Sea shelf break opposes variability of the surface winds on decadal timescales. For example, eastward wind anomalies typically coincide with a slower undercurrent. Silvano et al. (2022) hypothesised that this was due to on-shelf wind stress curl variability producing Ekman upwelling and downwelling anomalies that raise and lower isopycnals on the continental shelf. The suggestion was then that this leads to baroclinic anomalies at the shelf break that outweigh the barotropic effects of the shelf-break winds. In this section we consider the surface stress curl outputted by the ocean model used in this study, which accounts for sea ice and ocean currents.

Fig. S1a shows the time-mean surface stress curl, while Figs. S1b,c show composite anomaly responses of the surface stress curl using the undercurrent as predictor. These composites exhibit little clear spatial dependence, and do not obviously imply the existence of a physical link between the surface stress curl and the undercurrent. We may average the surface stress curl over the continental shelf (over the shelf region shown in Fig 3a of the main text) to ascertain whether, on average, the wind stress curl has the sign required for it to be the driver of the diagnosed decadally varying baroclinicity. For eastward undercurrent anomalies, during which cross-slope baroclinicity is large, we find that the sign of the area-averaged on-shelf anomaly is opposite to that required. That is, on average, the associated Ekman velocity anomaly is upward, which would be expected to raise on-shelf isopycnals and reduce the cross-shelf break baroclinicity. This leads us to conclude that surface stress curl variability is not responsible for the decadal variability of the undercurrent. Instead, results that we present in the main text show that sea-ice and ice-shelf freshwater fluxes are responsible.

Text S2

In this section we utilise the MITgcm configuration introduced by Haigh, Holland, and Jenkins (2023) to simulate the mechanism by which freshwater fluxes drive undercurrent variability in an idealised configuration. The model includes no ice shelves, sea ice or icebergs. This model uses a highly simplified forcing and geometry, summarised in Fig. S2. The domain (Fig. S2a) is a zonally re-entrant channel with continental shelf bathymetry which is 1000 m deep in the north and 500 m deep in the south, separated by a steep continental shelf slope. Walls on the continental shelf outline an embayment similar to the real Amundsen Sea. On the eastern side of the shelf slope we include a 700 m-deep trough and to its east a 400 m-deep ridge. As discussed in Haigh et al. (2023), these bathymetric features help to induce a deep cyclonic circulation on the continental shelf, as is simulated in the regional model.

The model is forced by a steady wind (Fig. S2a) that is motivated by actual time-mean winds over the Amundsen Sea. The wind is westerly (easterly) to the north (south) of the continental shelf break, and zero above the continental shelf slope. The wind speed extrema of 4 m s^{-1} is attained at the northern and southern boundaries.

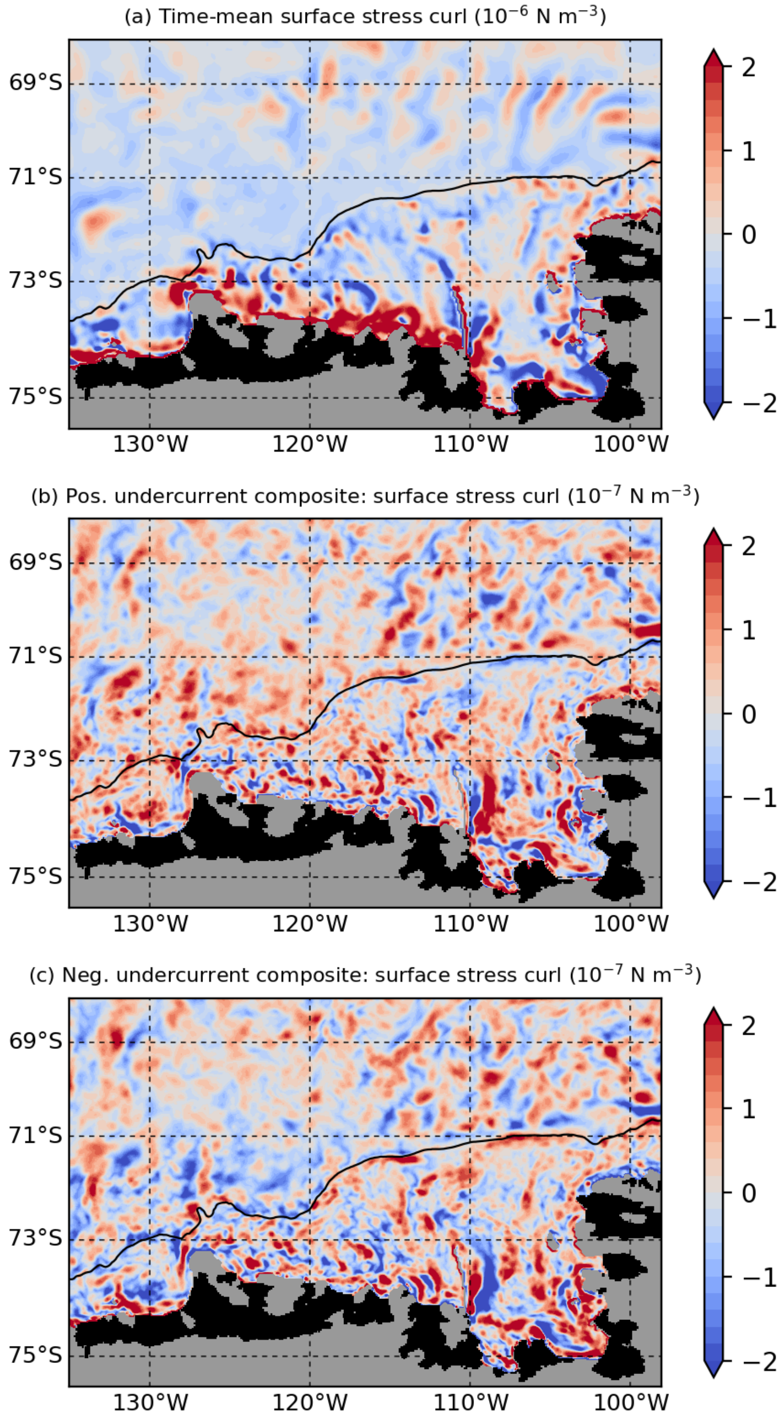

Figure S1. (a) Time-mean surface stress curl (10^{-6} N m^{-3}). (b,c) Composites of surface stress curl anomaly (10^{-7} N m^{-3}) for eastward/westward undercurrent anomalies. In all panels, grey masking represents land, black masking represents the ice shelves, and the black contour represents the 1000 m shelf-break isobath.

Potential temperature θ and salinity S are relaxed at the northern and southern boundaries to the profiles shown in Fig. S2c. At the northern boundary the relaxation profile includes a thermocline/halocline between 100 m and 300 m depths, which separates cold and fresh surface waters from warm and saline deep waters (CDW).

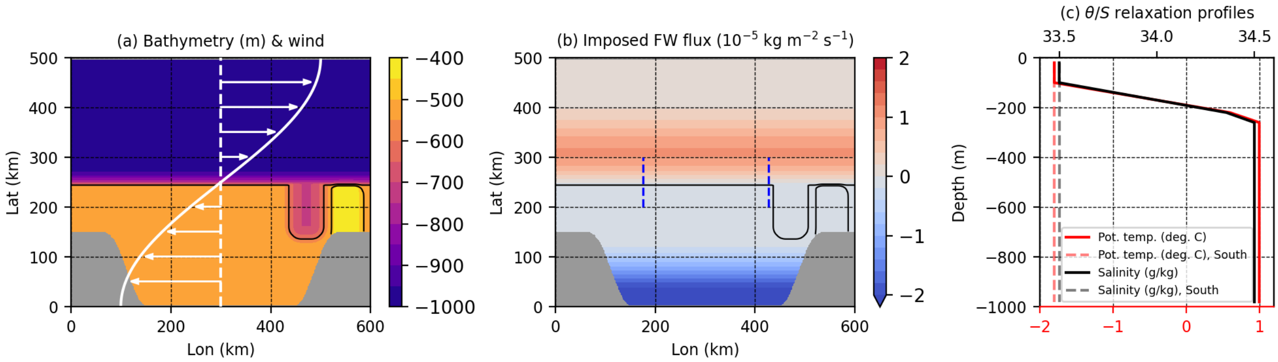

Figure S2. Setup of the idealised model. (a) Idealised model bathymetry (colour, m). Black contours represent the 500 m and 600 m isobaths. White arrows and contour represent the steady zonally uniform zonal wind measured relative to the white dashed line. The wind speed is zero over centre of the continental slope and is fastest with speed ± 4 m s^{-1} at the northern/southern boundary. (b) Spatial distribution of surface freshwater flux forcing (10^{-5} kg m^{-2} s^{-1}), which oscillates with 10-year period. This represents a time-mean evaluated over one positive phase of the forcing. (c) Relaxation profiles for potential temperature, θ (red), and salinity, S (black). Solid lines represent the profiles applied at the northern boundary with 10-day timescale and dashed lines represent the profiles applied at the southern boundary with 200-day timescale.

The timescale for the relaxation at the northern boundary is 10 days. At the southern boundary (Lat = 0 km) θ and S are relaxed towards -1.8°C and 33.5 g kg^{-1}, respectively. These values are also taken for the cold and fresh initial conditions used in model runs. At the southern boundary a 200-day relaxation timescale is used, significantly weaker than the relaxation at the northern boundary. This weak relaxation at the southern boundary is required for the model to maintain a realistic on-shelf heat distribution and realistic ASF at the shelf slope in steady state, since otherwise the shelf properties gradually drift warmer on centennial timescales. Haigh et al. (2023) found that wind-driven coastal downwelling at the southern boundary is not sufficient to maintain the ASF on these long timescales. At both the northern and southern boundaries the relaxation is switched off gradually over 4 grid points inward from the boundary.

Forced by the surface winds and θ/S relaxation, the model is spun up from rest for 40 years and is statistically stable after $\sim$ 20 years. The model is then restarted and run for a further 30 years with a freshwater flux applied at the surface which oscillates between positive and negative phases on a 10-year timescale. Fig. S2b shows the surface freshwater flux profile (a time-mean evaluated over the positive phase), which is motivated by composites from the regional model (main text Fig. 2d,f). In its positive phase the surface freshwater flux is positive (freshening) north of the shelf break and is negative (salinification) near the southern coast.

We use this surface flux to show that sea-ice freshwater fluxes alone are sufficient to drive decadal variability in the undercurrent that opposes the surface current. That is, we do not impose any variable ice-shelf melting and by extension we do not include the positive feedback effect that such melting would have on the undercurrent. The winds are held steady throughout the simulation.

Text S3

All output we show here is from the 30-year restart of the idealised model. Data is zonally averaged along the undercurrent section depicted in Fig. S2b. Fig. S3a shows depth-latitude plots of the time-mean density and zonal velocity. The model includes an ASF which is partially maintained by wind-driven downwelling at the southern boundary. A westward slope current sits above the ASF which transitions to an eastward undercurrent beneath the ASF due to thermal wind balance.

Fig. S3d shows timeseries of the along-slope surface current and undercurrent, both with 5-year running mean applied. Also shown is the time-dependence of the applied surface freshwater flux. The surface current and undercurrent are anticorrelated ($r = -0.60$, 99% significant), with the variable surface freshwater flux driving the same mechanism as in the regional model. The undercurrent response lags the freshwater flux with largest correlations ($r = -0.88$, 99% significant) diagnosed for a 2-year lag.

Fig. S3b,c shows composites of the density and along-slope velocity computed for undercurrent anomalies more than half of a standard deviation from the mean. The effect of the surface freshwater flux on the density is very similar to the regional model. The response to the off-shelf freshwater fluxes is concentrated in the upper 100 m of the water column, whereas the response to the on-shelf freshwater fluxes is spread through the entire 500 m depth. This is likely a consequence of the stratification being stronger off-shelf, which suppresses vertical mixing of salinity between the surface and deeper layers. The on-shelf response is weaker than in the regional model, but the total freshwater flux variability on the shelf is smaller in the idealised model as we do not include the contribution from the ice shelves.

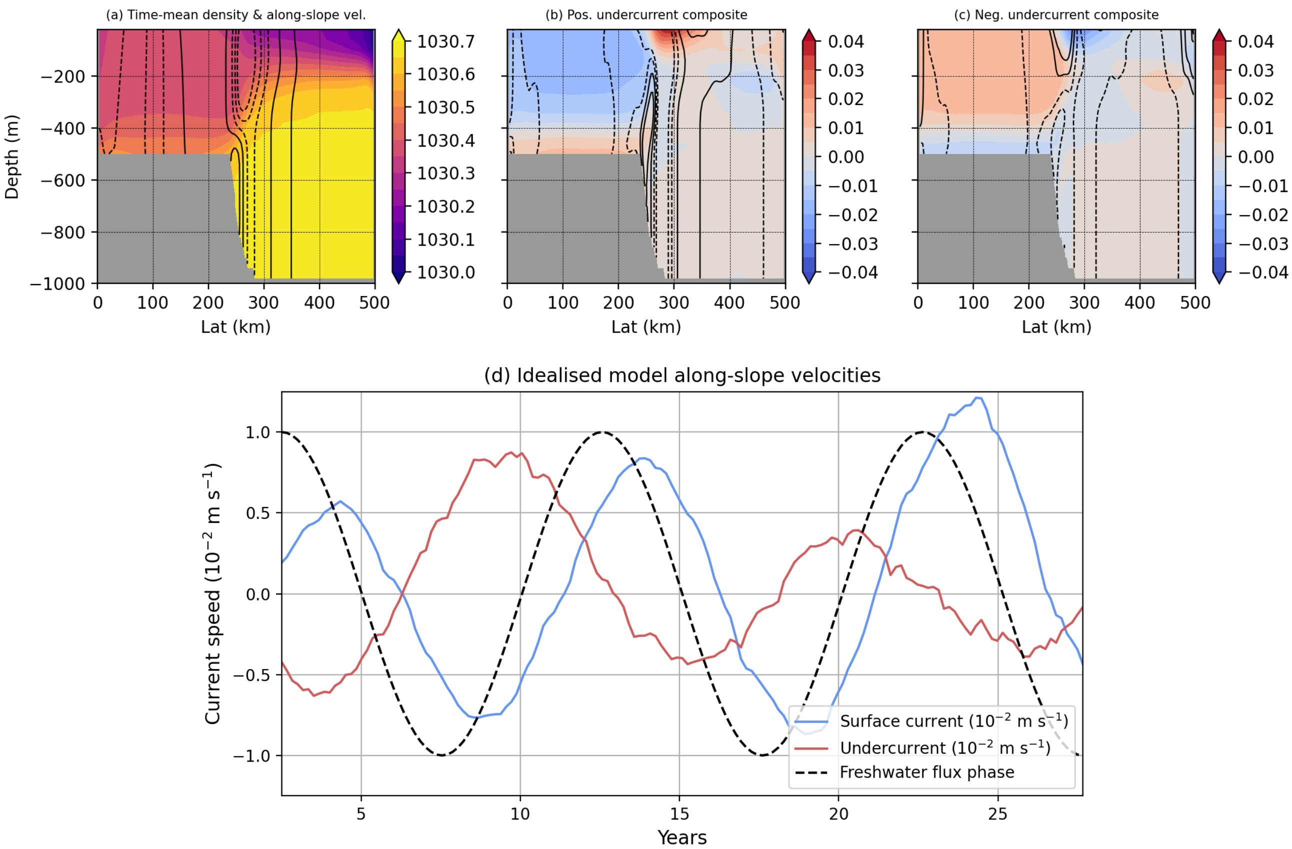

Figure S3. Idealised model outputs. (a) The time-mean, zonal-mean density (colour, kg m^{-3}) and zonal velocity (contours, 0.02 m s^{-1} contour interval). (b) Composites of the density (colour, kg m^{-3}) and zonal velocity (contours, 0.002 m s^{-1} contour interval) anomalies for eastward undercurrent anomalies. (c) The same as (b) but for westward undercurrent anomalies. (d) Timeseries of the surface current (blue, 10^{-2} m s^{-1}), undercurrent (red, 10^{-2} m s^{-1}) and time-dependence of the surface freshwater flux (black dashed). All zonal averages are evaluated along the section shown Fig. S2b. Timeseries have had 5-year running mean applied.

References

Haigh, M., Holland, P. R., & Jenkins, A. (2023, May). The Influence of Bathymetry Over Heat Transport Onto the Amundsen Sea Continental Shelf. *Journal of Geophysical Research: Oceans*, *128*(5). doi: 10.1029/2022jc019460

Silvano, A., Holland, P. R., Naughten, K. A., Dragomir, O., Dutrieux, P., Jenkins, A., ... Naveira Garabato, A. C. (2022, December). Baroclinic Ocean Response to Climate Forcing Regulates Decadal Variability of Ice-Shelf Melting in the Amundsen Sea. *Geophysical Research Letters*, *49*(24). doi: 10.1029/2022gl100646